remote sensing

MDPI

Article

From Satellite to Ground: An Integrated Multiscale and Multitemporal Remote-Sensing Workflow for Archaeological Prospection at Zar Tepe (1st–5th Centuries AD) in Surkhandarya, Uzbekistan

Jorge Angás [1,*], Paula Uribe [2], Verónica Martínez-Ferreras [3], Cristian Iranzo [4], Josep M. Gurt [3], Azamat Zakirov [5], Ilyas Yanbukhtin [5], Ulugbek Musaev [5], Enrique Ariño [6], Hikmatulla Hoshimov [7,8], Carlos Valladares [2] and Shakir R. Pidaev [9]

1 Department of Ancient Sciences and Institute of Heritage and Humanities (IPH), ARAID–University of Zaragoza, 50009 Zaragoza, Spain
2 Department of Ancient Sciences and Institute of Heritage and Humanities (IPH), University of Zaragoza, 50009 Zaragoza, Spain; uribe@unizar.es (P.U.); cvalladares@unizar.es (C.V.)
3 Departament d'Història i Arqueologia, Facultat de Geografia i Història, Universitat de Barcelona, 08001 Barcelona, Spain
4 Department of Geography and Spatial Management-Environmental Sciences Institute (IUCA), University of Zaragoza, 50009 Zaragoza, Spain; c.iranzo@unizar.es
5 Department of Archaeological Geophysics, Institute of Anthropology, Academy of Sciences of the Republic of Uzbekistan, Tashkent 100047, Uzbekistan; azamat.sh.zakirov@gmail.com (A.Z.); ilyas9348702@gmail.com (I.Y.)
6 Departamento de Prehistoria, Historia Antigua y Arqueología, Facultad de Geografía e Historia, Universidad de Salamanca, 37008 Salamanca, Spain
7 Department of Stone Age Archaeology of the Samarkand, Institute of Archaeology Named After Ya. Gulomov Under Agency of Cultural Heritage of the Republic of Uzbekistan, Samarkand 140305, Uzbekistan
8 Silk Road International Research Institute, Silk Road International University of Tourism and Cultural Heritage, Samarkand 140104, Uzbekistan
9 Institute of Fine Arts, Academy of Sciences of the Republic of Uzbekistan, Tashkent 100029, Uzbekistan
* Correspondence: j.angas@unizar.es

Highlights

What are the main findings?

- A comprehensive, integrated multiscale–multitemporal remote-sensing approach (CORONA, WorldView-3, UAV imagery, GNSS-PPP, and magnetometry) refined the reconstruction of the urban layout and identified productive areas at the Zar Tepe archaeological site (Uzbekistan).
- Multi-sensor analysis revealed previously undocumented features and refined the interpretation of sectors known from 20th-century excavations, including an orthogonal urban layout expressed as street-like linear alignments and building blocks, together with strong magnetic anomalies consistent with combustion-related and artisanal/production activity areas.
- Targeted shallow test excavations confirmed kiln-related remains and storage features, while additional magnetic and remote-sensing anomalies suggest possible domestic or activity-related structures that require further stratigraphic verification.

What are the implications of the main findings?

- The integration of satellite and UAV remote sensing with GNSS-PPP georeferencing and magnetic prospection provides an evidence chain to detect, prioritize, and validate archaeological targets through shallow, targeted ground-truth excavations (limited to superficial levels), optimizing field strategies and resource allocation.

Check for updates

Academic Editor: Massimiliano Pepe

Received: 7 May 2026
Revised: 12 June 2026
Accepted: 22 June 2026
Published: 26 June 2026

Copyright: © 2026 by the authors. Licensee MDPI, Basel, Switzerland. This article is an open access article distributed under the terms and conditions of the Creative Commons Attribution (CC BY) license.

- The combined satellite-to-ground workflow offers a scalable, transferable, and replicable framework for archaeological prospection, documentation, interpretation, and site management in Central Asia and other arid landscapes where large-scale excavation is constrained.

Abstract

Remote sensing has become a key non-invasive tool in archaeological prospection, particularly in regions where logistical constraints limit sustained fieldwork. This study presents the results from Zar Tepe (1st–5th centuries AD), in the Surkhandarya province of southern Uzbekistan, within northwestern Bactria. The research aimed to document the site's urban layout, accurately relocate Soviet-era excavation sectors within the present-day topography, and refine the interpretation of earlier interventions that were only partially documented and lacked precise georeferencing. A multiscale and multitemporal methodology was applied, integrating CORONA and WorldView-3 satellite imagery, UAV and terrestrial photogrammetry, GNSS Precise Point Positioning, magnetic prospection, and targeted archaeological verification. The workflow followed an iterative laboratory–field sequence, combining remote-sensing analysis, field checks, data refinement, and systematic ground-truth validation. Fieldwork was conducted during two contrasting phenological periods, in June 2024 and December 2025, to assess seasonal variability in surface and subsurface visibility. The integrated approach enabled the accurate spatial fitting of legacy excavation sectors and supported the cross-validation of optical and salt-efflorescence-related anomalies with geophysical evidence. These results provide a stronger basis for the cautious interpretation of buried architectural features and for refining hypotheses concerning Zar Tepe's urban organization and occupational dynamics.

Keywords: Central Asian archaeology; archaeological remote sensing; historical satellite imagery; WorldView-3; multisensor data integration; GNSS Precise Point Positioning (PPP); magnetic prospection; arid landscapes; salt-efflorescence soil marks; web GIS

1. Introduction

Zar Tepe—often translated as "Golden Hill" based on its toponymic components—is an archaeological site dated to the Kushan and Kushan–Sasanian periods (1st–5th centuries AD), situated in the Surkhandarya province of southern Uzbekistan, within the northwestern sector of ancient Bactria (Figure 1). The Kushan period in Bactria (1st–3rd centuries AD) has been widely described as a phase of political stability and economic prosperity, reflected in the growth of valley settlements and the architectural complexity of urban centers [1,2]. Trade intensified at local, regional, and interregional scales along the Silk Roads, through maritime and overland routes linking the Indus region, the Tarim Basin and China, Arabia, the Near East, and the Mediterranean [3]. Kushan rulers promoted religious diversity and played a key role in the diffusion of Buddhism across Central Asia, fostering monastic foundations and a distinctive artistic tradition that combined local, Hellenistic, Iranian, and Eastern influences. From the mid-3rd century AD onward, northern Bactria entered the Sasanian sphere of influence, followed by the arrival of nomadic Hunnic groups during the 4th–5th centuries AD [1,4–7].

The broader region is characterized by a vast irrigated plain extending north of the Hindu Kush, watered by the Amu Darya (ancient Oxus River) and its tributaries, particularly the Surkhandarya. This area is characterized by a markedly continental climate and extreme summer temperatures that can exceed 40 °C. In arid settings, evaporation

and capillary rise may promote salinity-related surface processes, a phenomenon widely documented in Uzbekistan's irrigated landscapes [8].

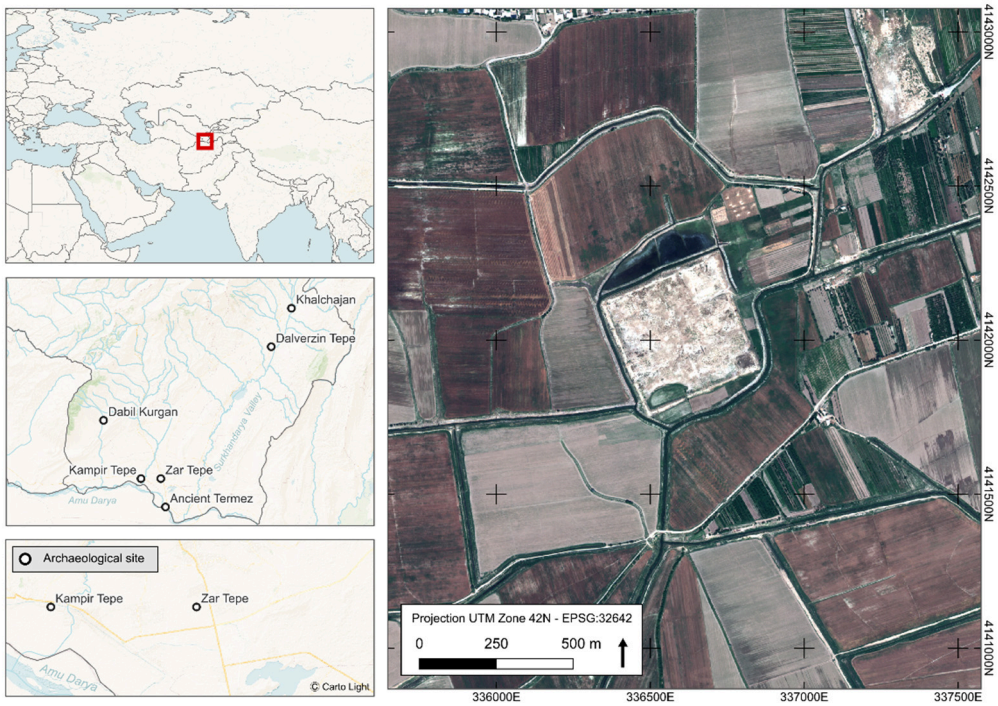


Figure 1. Map of northern Bactria showing the location of Zar Tepe and other sites in southern Uzbekistan, and WorldView-3 satellite image of Zar Tepe acquired on 29 May 2017.

The Surkhandarya Valley contains numerous archaeological settlements from different periods, with a particularly high density of sites dating to the Kushan era, broadly contemporaneous with the Roman period. Whereas Termez and Dalverzin Tepe appear to have functioned as the main urban centers of the valley, owing to their size and the importance of the remains associated with Buddhist complexes [2], Zar Tepe represents one of the many smaller settlements distributed along the irrigation channels of the alluvial plain. Roughly square in plan (~400 m per side; ~16.9 ha), it consists of a fortified enclosure bounded by a defensive wall and an external ditch (Figure 2). The site lies approximately 36 km northeast of ancient Termez, within the broader regional landscape of other major Kushan-period sites such as Dalverzin Tepe and Kampir Tepe (Figure 1). This broader regional framework and its long-term urban dynamics have recently been examined at ancient Termez through an integrated approach combining excavation, survey, and remote sensing data (CORONA and WorldView-3). This research has highlighted the role of irrigation and geomorphic processes in shaping site visibility and preservation [9]. The first excavations at Zar Tepe began in 1950. They were carried out by L.N. Albaum, although the results of these interventions were never published. Between 1972 and 1986, the site was systematically excavated by various teams of Soviet archaeologists [10] (Figures 3 and 4). The results of these investigations were published in articles and book chapters as the excavations progressed (Table 1). The sequence of occupation, material culture, and several aspects of the domestic architecture at Zar Tepe are relatively well documented. However, a comprehensive georeferenced plan of the urban space integrating all excavated structures has so far been lacking. Although the Soviet-era interventions were compiled in a later published plan, their precise spatial relocation within the site's current topography remained unresolved. The most recent and comprehensive publication on Zar Tepe presents the results of investigations conducted in sectors 6, 9, 12, and 13 [10]. In this context, a major contribution of the present study is the

georeferencing and spatial integration of the areas excavated and documented in previous archaeological interventions.

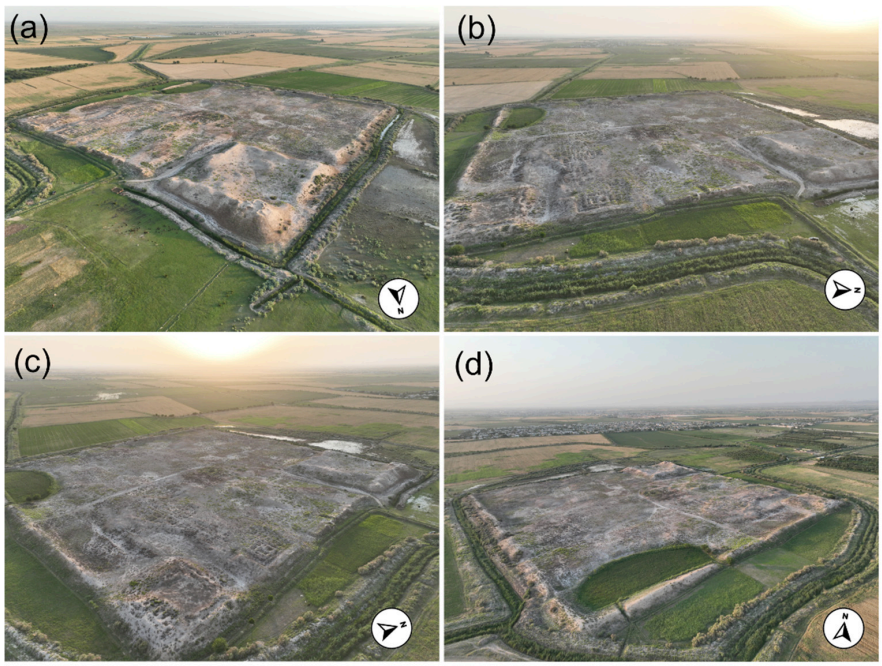


Figure 2. Oblique aerial views of the archaeological site of Zar Tepe acquired at sunset: (**a**) view oriented to the southwest toward the Amu Darya River; (**b**) view oriented to the west; (**c**) view oriented to the northwest; and (**d**) view oriented to the north.

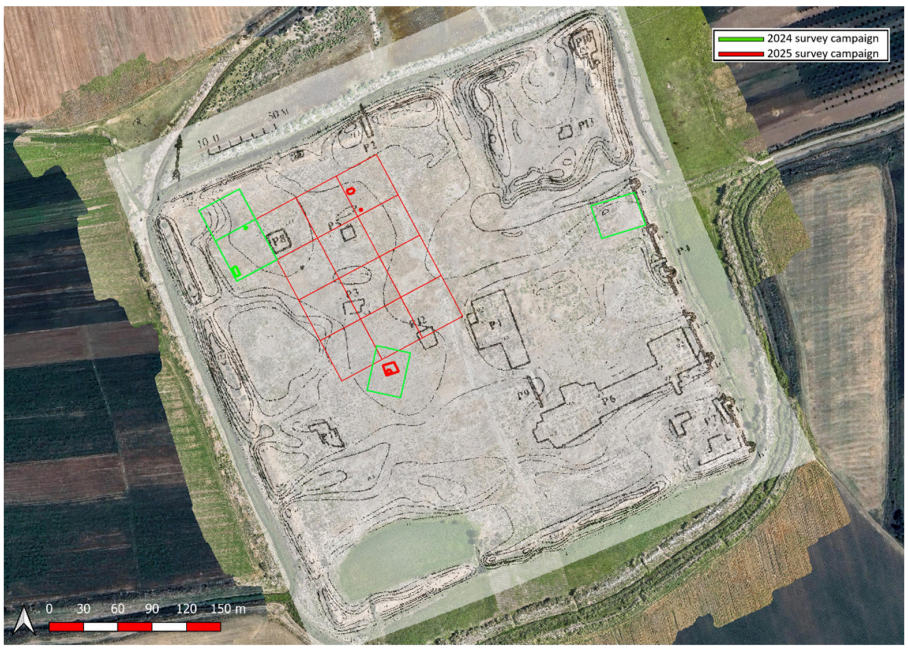


Figure 3. General plan of Zar Tepe, based on the published archaeological documentation by Zavyalov [10], showing the spatial distribution of excavation sectors (P, *raskop*) opened during the Soviet-era investigations (1950s–1980s), as well as the survey areas investigated during the 2024 and 2025 Uzbek–Spanish campaigns. These legacy and newly documented sectors were georeferenced and spatially fitted to the present-day topography using UAV photogrammetry and GNSS-PPP control.

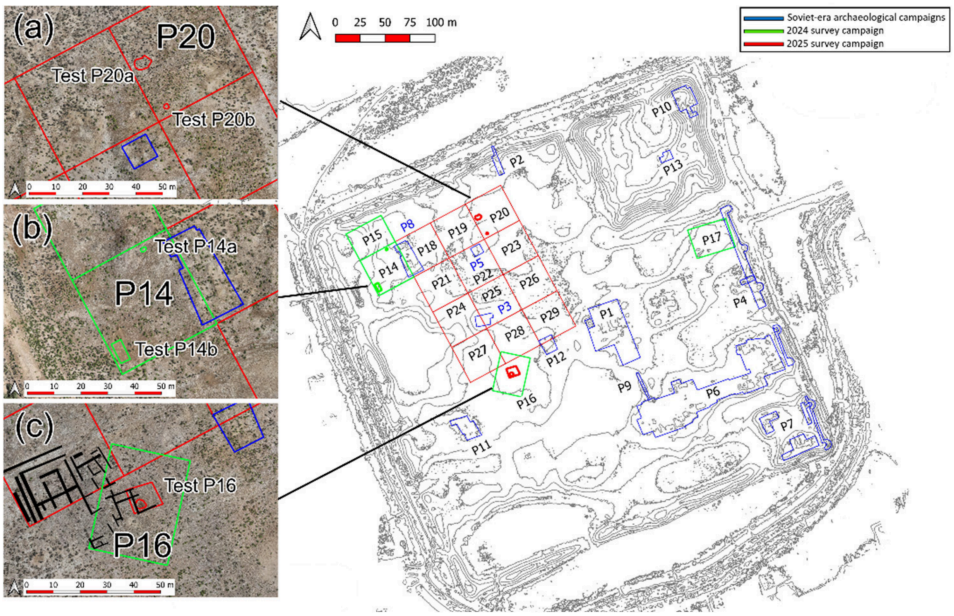


Figure 4. Schematic overview of the spatial distribution of the sectors documented at Zar Tepe—Soviet-period excavation sectors P1–P13 (blue), sectors investigated during the 2024 campaign P14–P17 (green), and sectors analyzed during the 2025 campaign P18–P29 (red)—overlaid on the site-wide topographic model generated in 2024–2025 by the Uzbek–Spanish project. Enlarged views (**a**–**c**) from the general plan illustrate the different archaeological test excavations undertaken during the 2024 (P14a, P14b) and 2025 (P20a, P20b, P16) field campaigns.

Soviet work particularly documented a defensive system with semicircular bastions (e.g., seven towers along the eastern wall spaced ~34 m apart) and multiple entrance gates connected to an orthogonal street grid [2,10,11] (Figure 4). Excavations within the enclosure revealed parts of the urban layout, including public buildings and a fortified citadel (P10; P13) in the northern sector (approx. 120 m per side), built on an artificial platform and isolated by its own moat (Figure 2). These studies established occupation between the 1st and 5th centuries AD. Evidence of Buddhist activity is provided by a sanctuary and a small stupa, which forms part of a Buddhist sanctuary located about 300 m northeast of the east-northeast face of the Zar Tepe defensive wall [12]. The stupa's late 3rd-century AD reliquary contained coins of later Kushan rulers and ivory objects. The ceramic assemblages were notable and showed affinities with ceramics from Termez and other Kushan-period Bactrian sites.

The most recent study dates the occupation of the site to between the 1st and 5th centuries AD, although there are indications of an earlier occupation phase, dated to the 1st century BC, associated with the Yuezhi settlement [10]. The data obtained from the site suggest that Zar Tepe was among the most significant economic, productive, and commercial centers in the Surkhandarya Valley and northern Bactria, and also served as one of the Buddhist centers in the region.

Following Soviet-era investigations, research at Zar Tepe was discontinued for several decades. In 2022, an Uzbek–Spanish team launched a new research initiative within the framework of the IPAEB team (International Pluridisciplinary Archaeological Expedition to Bactria), in collaboration with Uzbek partner institutions, namely the Institute of Fine Arts, Academy of Sciences of the Republic of Uzbekistan, the Laboratory of Geophysics and Nanomineralogy (Center for Advanced Technologies, Tashkent), and the Samarkand Institute of Archaeology named after Ya. Gulomov (under the Agency of Cultural Heritage of the Republic of Uzbekistan) and Silk Road International University of Tourism and Cultural Heritage. The project was funded by the Spanish Ministry of Science and

Innovation and the Spanish Palarq Foundation. The overarching objective is to enhance knowledge of Zar Tepe and, more broadly, of Kushan-period urban centers in ancient Bactria, with a particular focus on ceramic production areas and their long-term urban dynamics. This objective is addressed through an innovative multiscale and multitemporal methodological approach that combines remote sensing and geomatic analysis, building on previous research experience in ancient Termez. Besides the application of a wide range of archaeological methods including stratigraphic archaeological excavations, terrestrial and geophysical surveys, and photogrammetry for 3D recording [9,13–21], a multiscale and multitemporal remote sensing approach was conducted at ancient Termez by combining excavations, survey, and remote sensing (CORONA and WorldView-3). This research highlighted the role of irrigation and geomorphic processes in shaping site visibility and preservation [9].

An earlier implementation of the multiscale methodological framework previously tested at ancient Termez produced promising results and provided a useful basis for its application at Zar Tepe [20,21]. A preliminary satellite-based study specifically focused on Zar Tepe was subsequently published by Iranzo et al. [22], in which CORONA, HEXAGON, and WorldView-3 imagery were processed to evaluate the automated generation of derived products, including spectral indices, PCA outputs, high-pass-filtered historical imagery, and a web-based tool for the visual identification of cropmarks and potential buried urban structures. That contribution provided the initial remote-sensing cartographic basis for Zar Tepe and helped define areas of interest for subsequent fieldwork. However, it was conceived as a preliminary methodological and satellite-based assessment, prior to the systematic ground verification of the detected anomalies.

Building on this preliminary satellite-based framework, the present paper incorporates a broader multi-sensor and field-validated dataset that substantially expands the scope, evidence base, and archaeological interpretation of the previous work. This new phase included two joint field campaigns combining GNSS-PPP georeferencing and stakeout, geomagnetic survey, aerial and terrestrial photogrammetry, and targeted archaeological test excavation. The campaigns were deliberately conducted under contrasting phenological and environmental conditions: a summer campaign (9–18 June 2024), coinciding with peak aridity and minimal vegetation cover, and a winter campaign (8–13 December 2025), characterized by higher soil moisture and different surface responses. This dual-season strategy was adopted to improve the detection, verification, and interpretation of archaeological features by exploiting complementary environmental conditions observable through both remote sensing and ground-based survey.

As a first step, we aim to accurately relocate, georeference, and spatially reconstruct the areas previously investigated through earlier excavations within the site's present-day topography (Table 1), thereby achieving a more precise topographic reconstruction of previous archaeological work, and to assess—using the remote-sensing and geomatic techniques applied here—whether additional, previously unrecognized areas can be detected. Specifically, we aim to: (i) document and analyze the site's urban organization—including the defensive system, public and residential areas, and artisanal sectors—and its relationship with the surrounding physical landscape using a multiscale and multitemporal satellite-based approach; (ii) refine the interpretation of previously excavated areas by integrating remote-sensing evidence with magnetic prospection and field verification, with particular attention to earlier archaeological interventions that were only partially documented and lacked accurate georeferencing; and (iii) identify potential ceramic production areas or other artisanal spaces not clearly recognized in previous research, based on anomalies detected in multisource datasets.

Table 1. Chronological overview of archaeological research at Zar Tepe, listing the investigated sectors (P), responsible research teams, and types of interventions conducted during the Soviet period.

Archaeological Campaign/Director	Date	Excavated Sector(s) (P)	Publications
L.I. Albaum	1950–1952	On the highest hill, east-northeast sector	Unpublished
Bactrian Expedition of the Leningrad Institute of the USSR Academy of Sciences (Bakstriyskoy Ekspyeditsyyey LOIA AN SSSR)	1972	P1 (Raskop 1)	Shchetenko (1974) [23]
K.S. Sabirov and V.N. Pilipko	1972	P2 (Raskop 2)	Sabirov and Pilipko (1974) [24]
V.N. Pilipko	1973	P2 (Raskop 2)	Pilipko (1976) [25]
V.A. Zavyalov and V.I. Osipov	1973	P3 (Raskop 3)	Zavyalov and Osipov (1976) [26]
K.S. Sabirov	1973–1974	P4 (Raskop 4)	Sabirov (1976) [11]
V.M. Masson	1974	Not labelled	Masson (1974) [27]
V.M. Masson	1974	P5 (Raskop 5)	Unpublished
V.A. Zavyalov	1975–1986	P6 (Raskop 6)	Zavyalov (1979) [28] Zavyalov (1981) [29] Zavyalov and Galibin (1990) [30] Zavyalov (1993) [31] Abdullaev and Zavyalov (1985a) [32] Abdullaev and Zavyalov (1985b) [33] Zavyalov (2008) [10]
G.A. Koshelenko, Institute of Academy of Sciences of the USSR and Moscow State University M. V. Lomonosov (IA AN SSSR i MGU im. M.V. Lomonosova)	1976–1978	P1 (Raskop 1)	Unpublished
Sh. Pidaev	1977	P7 (Raskop 7)	Pidaev (1990) [34] Reutova (1986) [35]
Sh. Pidaev	1977	P8 (Raskop 8)	Pidaev (1988) [36]
V.A. Zavyalov	1978	P9 (Raskop 9)	Zavyalov (2008) [10]
T.D. Annaev, Institute of Archaeology of the Academy of Sciences of the Uzbek Soviet Socialist Republic, SAK'E Expedition (IA AN UzSSR, Ekspyeditsiya SAK'E)	1979–1981	P10 (Raskop 10)	Abdullaev and Annaev (1990) [37]
T.D. Annaev, Institute of Archaeology of the Academy of Sciences of the Uzbek Soviet Socialist Republic (IA AN UzSSR, Ekspyeditsiya SAK'E)	1981–1982	P11 (Raskop 11)	Unpublished
V.A. Zavyalov	1985	P12 (Raskop 12)	Zavyalov (2008) [10]
V.A. Zavyalov	1986	P13 (Raskop 13)	Zavyalov (2008) [10]

2. Materials and Methods

The methodological design of this study was based on the progressive integration of historical satellite imagery, contemporary very-high-resolution optical data, UAV-derived photogrammetric products, GNSS-PPP geodetic control, geomagnetic prospection, targeted archaeological test excavation, and GIS-based data management. Rather than treating these datasets as independent sources of information, the workflow was conceived as a cross-validation sequence in which each analytical step informed the next: satellite imagery supported the initial detection of potential archaeological anomalies; UAV documentation refined their spatial expression at higher resolution; GNSS-PPP provided a common geodetic framework; magnetometry tested their subsurface expression; and targeted excavation supplied ground-truth evidence for selected features.

To clarify the role of each dataset within this integrated workflow, Table 2 summarizes the acquisition context, spatial or sampling resolution, processing procedures, archaeological purpose, and validation strategy adopted at Zar Tepe. This overview also serves as a methodological bridge between the remote-sensing phase and the subsequent field-based

verification procedures described in the following sections. A schematic representation of the complete methodological workflow is provided in Appendix A, Figure A1.

Table 2. Overview of the multiscale and multitemporal datasets integrated in the Zar Tepe workflow, including acquisition dates, spatial or sampling resolution, processing procedures, archaeological purpose, and validation strategy.

Dataset/Source	Date/Campaign	Resolution/Spatial Unit	Main Processing	Archaeological Role/ Validation
CORONA/HEXAGON	1969–1978	c. 0.6–1.8 m	Georeferencing; high-pass filtering	Historical baseline; GIS comparison with Soviet-era plans and modern datasets
WorldView-3	2017–2021	0.31 m PAN; 1.24 m MS	BOA correction; pansharpening; PCA; spectral indices	Spectral anomalies, cropmarks, soil marks; cross-checking with UAV and magnetometry
UAV photogrammetry	June 2024	1.04–1.88 cm/pixel	SfM; orthomosaics; dense clouds; DTM	Microrelief, excavation scars, salt-related soil marks; validated with GCPs/GNSS
Terrestrial photogrammetry	2024–2025	c. 1 mm/pixel	Close-range SfM; detailed orthophotos; 3D models	Documentation of test pits, kiln-related remains, and storage features
GNSS-PPP	2024–2025	<4 cm	Stakeout; GCPs; grid layout; topographic recording	Unified geodetic reference system for all datasets (WGS 84/UTM zone 42N, EPSG:32642)
Magnetometry	2024–2025	0.25 × 0.25 m grid	Geoplot processing; interpolation; anomaly mapping	Detection of anomalies verified by test pits
Test excavations	2024–2025	P14a, P14b, P16, P20	Shallow stratigraphic testing; photogrammetry; GIS integration	Ground-truth validation of remote-sensing and magnetic anomalies
DiGHER/GIS	2024–ongoing	Multiscale	Web mapping; 3D point-cloud management	Data integration, traceability, interpretation, and future planning

2.1. Multitemporal Satellite Integration and Image Correction for Archaeological Prospection

The integration of declassified historical imagery with contemporary high-resolution satellite data provides a powerful basis for assessing landscape dynamics and archaeological proxies across multiple temporal scales. This perspective is particularly relevant at Zar Tepe, where a central research challenge is the relocation and spatial fitting of Soviet-era excavation areas within the site's present-day topography, while also evaluating the potential for detecting additional, previously unrecognized archaeological zones beyond the historically explored sectors. To address this, the preliminary remote-sensing framework was conceived as an integrative, geomatics-driven approach designed to align heterogeneous datasets (e.g., historical satellite imagery, modern satellite products, UAV-derived models, and geophysical survey grids) within a consistent spatial reference system, thereby enabling robust comparison, cross-validation, and interpretation.

Accordingly, the remote-sensing methodology applied to Zar Tepe combined two complementary categories of satellite data, each offering distinct spectral characteristics and interpretive advantages.

First, declassified historical imagery from the CORONA and HEXAGON programs (1960s–1970s) was employed. CORONA has underpinned a wide range of archaeological studies by preserving a high-resolution record of the Earth's surface several decades prior to major anthropogenic transformations. In arid and semi-arid regions, this archive fre-

quently reveals surface expressions that are now obscured by burial, inundation, erosion, or modern land use, and it has therefore become a standard resource for remote-sensing-based archaeological prospection and landscape analysis [38,39]. Owing to its near-global coverage and, in many cases, stereoscopic potential prior to major landscape transformations, CORONA is particularly valuable for reconstructing past landscape configurations and establishing interpretive baselines for comparison with modern observations [20,21,40]. Collectively, these studies emphasize CORONA not simply as a source of historical imagery, but as a spatially explicit record that supports the reconstruction of former landscapes and enhances the reliability of archaeological interpretation in regions affected by intensive land-use change. In Central Asia, similar diachronic remote-sensing approaches integrating historical imagery, field survey, and landscape-scale assessment have also proven effective in the Samarkand region [41]. In northern Bactria, a comparable multitemporal strategy integrating CORONA and WorldView-3 has proven effective for reconstructing urban layouts and assessing landscape change at ancient Termez, serving as a relevant methodological parallel for the Surkhandarya valley [9]. For Zar Tepe specifically, these declassified datasets provide a baseline predating decades of agricultural intensification and landscape modification in the Surkhandarya valley, offering privileged access to spatial patterning that may be partially masked in the modern terrain.

Second, contemporary WorldView-3 (WV3) high-resolution satellite imagery provides radiometrically rich and spatially detailed representations of current surface conditions. At Zar Tepe, these datasets support the detection of subtle archaeological proxies through enhanced spatial detail and spectral contrast, while also bridging the historical baseline with present-day ground verification. More importantly, the combined use of historical and contemporary imagery enables the discrimination of persistent archaeological patterns from transient surface effects, the evaluation of landscape change influencing feature visibility, and the prioritization of targets for subsequent non-invasive survey strategies, including UAV-based mapping, geophysical prospection, and focused ground verification.

Within the broader workflow summarized in Table 2, the multiscale satellite-based analysis relied specifically on the following cartographic and remote-sensing datasets:

- Archaeological site planimetries derived from previous excavations and published literature [10,23–26,36], which were interpreted and georeferenced within a web-based GIS environment.
- High spatial resolution multispectral and multitemporal satellite imagery, primarily from the CORONA satellite program (12 November 1973; 11 June 1975; 28 January 1976) and WorldView-3 (WV3; May 2017, August 2017, December 2018 and January 2021). These datasets, acquired under contrasting seasonal and phenological conditions, were processed using Principal Component Analysis (PCA) and vegetation indices to enhance the detection of subsurface archaeological features, support topographic reassessment of the surveyed areas, and verify anomalies identified in the investigated sectors.

To ensure comparability across multi-date and multi-sensor observations, remote-sensing data must undergo correction procedures that minimize radiometric and geometric inconsistencies attributable to acquisition conditions, sensor characteristics, and temporal variability [42]. In archaeological contexts, accurate spatial positioning is particularly critical, as it allows seamless integration with complementary datasets, such as geophysical measurements and UAV-derived products, at the scale required for interpretation and field validation. Consequently, the fusion of satellite imagery with independent sources of evidence is increasingly common in archaeological research [43], since convergent signals from different sensors reduce ambiguity and allow hypotheses to be formulated and tested more explicitly.

In practice, many sensors distribute imagery using predefined compression parameters and often lack a complete set of radiometric and geometric pre-processing steps, requiring end users to perform these procedures. Under these conditions, additional processing is required to obtain data suitable for scientific analysis. In this study, we developed a streamlined and reproducible set of routines for (i) image correction and co-registration, (ii) the generation of derived channels aimed at enhancing spatial detail and improving the interpretability of historical panchromatic imagery [44] and (iii) the integration of all corrected and derived datasets into a georeferenced GIS framework to support spatial analysis, cross-validation, and archaeological interpretation. Ultimately, this preliminary correction-and-integration phase is not an isolated technical step: it directly underpins our ability to (i) reposition and reassess the spatial logic of previously excavated areas within the current topography, and (ii) expand archaeological understanding beyond known sectors by identifying new target zones for geophysical prospection and ground verification based on coherent, multisource anomaly patterns.

2.1.1. Satellite Data Pre-Processing: CORONA, HEXAGON, and WorldView-3

The satellite datasets used in this study required different preprocessing strategies due to their distinct acquisition characteristics, spatial resolutions, and historical contexts.

Historical satellite images from the CORONA and HEXAGON programs (1960s–1970s) were incorporated to document the archaeological landscape prior to major anthropogenic and natural transformations. Despite their relatively modest spatial resolution—approximately 1.8 m in most CORONA scenes, and up to 0.6–1.2 m in selected cases—these datasets offer an exceptional baseline for identifying changes related to agricultural intensification, infrastructure development, or natural processes [20,21]. Because these historical images lack an inherent spatial reference system, geometric correction and georeferencing processes were applied as initial steps. Using the Georeferencer plugin in QGIS, a set of 22 evenly distributed ground control points (GCPs) was defined on stable landscape elements such as road intersections, irrigation channels, river crossings, and permanent constructions (Figure 5). A second-order polynomial transformation was computed, and pixel values were resampled using bilinear interpolation.

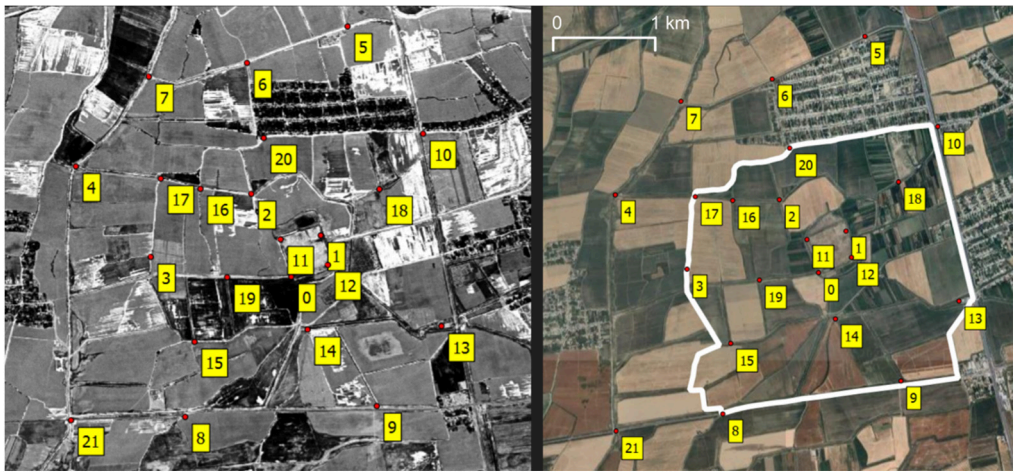


Figure 5. Distribution of the different GCPs used to georeference the frame DS1110-1040DF018-B. On the left, the original CORONA image, on the right, over the Google Satellite Imagery and the Zar Tepe area of interest (in a white border).

The georeferencing step was performed by defining an empirical model using a second-order polynomial and a bilinear resampling method, with ground control points (GCPs) placed close to the digitized area of interest around Zar Tepe (Figure 5). Depending on the

CORONA frame, between 15 and 22 GCPs were used during the georeferencing process (Table 3). The resulting mean errors ranged from 3.6 to 8.5 pixels, most likely reflecting film distortions associated with the original satellite missions [45].

Table 3. Parameters of the georeferencing process for the CORONA frames used in the study, including the mean error in pixels and the number of GCPs.

Image ID-Frame	Date	Mean Error (Pixels)	Number of GCPs
DS1107-2298DA079-D	11 August 1969	5	15
DS1109-2234DF042-B	20 March 1970	5.09	17
DS1110-1040DF018-B	23 May 1970	3.63	22
DS1110-1137DA036-B	29 May 1970	4.62	17
DS1110-1137DF030-C	29 May 1970	5.24	15
DS1112-1040DA119-D	21 November 1970	3.85	16
D3C1207-100019A030	12 November 1973	5.61	18
D3C1210-100016A048	11 June 1975	8.53	19
D3C1211-300348A045	28 January 1976	7.11	22
D3C1214-100095A044	25 March 1978	4.89	21

High-resolution multispectral imagery acquired by the WorldView-3 (WV3) satellite was used to enhance the detection of subtle variations in vegetation and soil conditions associated with buried archaeological structures. WV3 imagery provides a spatial resolution of 0.31 m for the panchromatic band and 1.24 m for the multispectral bands. These data were subjected to radiometric and atmospheric correction to minimize atmospheric effects and ensure physical consistency across scenes. Digital numbers were first converted to top-of-atmosphere radiance and subsequently corrected to bottom-of-atmosphere reflectance using the Second Simulation of the Satellite Signal in the Solar Spectrum (6S) radiative transfer model; 6S is a radiative transfer model that simulates atmospheric radiative response and provides the parameters required to compute surface reflectance in VIS-NIR [46]. Previous studies have shown that 6S-based atmospheric correction can outperform simpler image-based approaches, often producing surface-reflectance estimates closer to field spectroradiometer measurements [47,48]. Topographic correction was not applied due to the flat terrain and the absence of significant relief or tall vegetation.

Following atmospheric correction, the spatial resolution of the WV3 multispectral imagery was enhanced through a pansharpening process. The multispectral bands were fused with the panchromatic band using the Bayesian fusion approach, as it provides improved preservation of spectral information and ensures continuity with the multitemporal image-enhancement strategy previously explored at ancient Termez [9]. Both Bayesian and other degradation-model-based fusion methods, as well as recent deep convolutional neural network (CNN) approaches, have demonstrated an optimal balance between spatial enhancement and spectral fidelity in remote sensing benchmarks [49,50].

Given the saline alluvial setting of the Surkhandarya valley, we considered that localized salt-related high-reflectance soil marks may alter multispectral contrast and influence the response of soil- and vegetation-sensitive indices. Consequently, index-based interpretations were not used in isolation but were systematically cross-checked against PCA outputs and independent geomagnetic evidence [51,52].

2.1.2. Satellite Data Post-Processing

The corrected and pansharpened imagery served as the basis for subsequent analytical processing. To enhance subtle variations in vegetation vigor, soil moisture, and surface composition potentially associated with buried archaeological remains, a set of neochannels was

generated from the WorldView-3 (WV3) data through spectral-index computation and Principal Component Analysis (PCA). This approach proved effective in highlighting patterns related to subsurface structures—such as walls, streets, and buildings—which can modify vegetation distribution and generate detectable cropmarks in satellite imagery. Principal components were derived using the DimensionalityReduction algorithm implemented in the Orfeo ToolBox. A total of 219 band combinations were analyzed, encompassing all possible combinations of WV3 spectral bands using a minimum of three input bands. For each band combination, the resulting output included the same number of principal components as input bands, capturing the dominant modes of variance within the selected spectral subset (Figure 6).

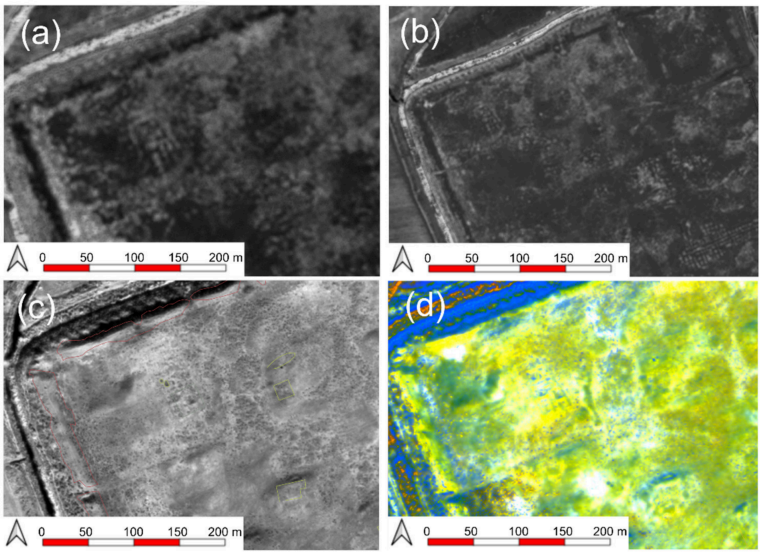


Figure 6. Processed WorldView-3 satellite imagery of the northwestern quadrant of Zar Tepe using vegetation/soil indices and Principal Component Analysis (PCA) to enhance subtle spectral contrasts potentially linked to buried archaeological features: (**a**) OSAVI (August 2017); (**b**) SAVI (May 2017); (**c**) NLI (January 2021); and (**d**) PCA component 14 (Coastal, Yellow and NIR bands) (December 2018).

Spectral indices were computed in an automated and fully reproducible manner based on a predefined list of index formulations. The selected indices are stored in a JSON file stored in the toolbox repository [53]. All near-infrared bands were treated equivalently and assimilated to the WV3 NIR1 band to ensure consistency across index calculations. This approach enabled the systematic generation of a comprehensive set of derived spectral features for subsequent analysis. The complete list of applied spectral indices, together with their mathematical formulations, is available in the published toolbox repository [53].

For the CORONA and HEXAGON declassified imagery, additional neochannels were generated using spatial high-pass filtering techniques to enhance fine-scale features such as roads, walls, building remains, and other subtle anthropogenic traces. High-pass filters emphasize abrupt spatial variations in pixel values and local contrast while suppressing low-frequency background information related to illumination effects or gradual terrain variations. As a result, these filters highlight archaeological features primarily expressed as edges, linear structures, and textural differences rather than absolute radiometric values.

Four widely used high-pass filters were selected based on their demonstrated effectiveness in archaeological and remote-sensing applications. These include the Laplacian filter, which enhances edges by computing second-order spatial derivatives; the Laplacian of Gaussian (LoG), which combines edge detection with noise suppression; the Sobel operator (horizontal kernel), which emphasizes directional gradients and linear features such as

roads; and the classical high-boost (unsharp masking) filter, which enhances fine spatial detail by amplifying high-frequency information.

2.2. Python Toolbox

A Python-based (v3.11) processing pipeline was developed to preprocess WorldView-3 (WV3) imagery and to generate neochannels. The workflow integrates tools from the Orfeo ToolBox (OTB) [54] and the Geospatial Data Abstraction Library (GDAL), combining their functionalities within a unified and automated framework. The final output of the pipeline consists of WorldView-3 (WV3) images corrected to bottom-of-atmosphere (BOA) reflectance, ensuring radiometrically consistent data suitable for further analysis. Beyond these corrected products, the pipeline generates a set of derivative datasets, including principal component analysis (PCA) images and multiple spectral indices computed from the WV3 multispectral bands (Figure 6). Furthermore, the workflow includes the application of a series of high-pass filtering techniques to historical CORONA panchromatic imagery, aimed at enhancing high-frequency spatial information relevant for archaeological feature detection [53].

2.3. Web-Based GIS Tool for Field Planning

Another key component of the study was the development of an interactive web-based tool. Built with modern web technologies—HTML, JavaScript, and the Leaflet library—the online viewer was created to allow intuitive exploration of georeferenced imagery and derived products. The viewer, designed with a simple and user-friendly interface, enables overlaying multiple information layers and extracting cropmarks in GeoJSON format, thereby supporting both field survey campaign planning and the geolocation and identification of features during fieldwork (Figure 7). In this way, this tool serves not only as a visual data repository but also as a collaborative platform for the Spanish–Uzbek research team, distinguishing the initial satellite-based identification phase in 2024 from the subsequent processing and analysis of orthophotographs generated in 2025.



Figure 7. Example of the web-based GIS mapping environment developed for Zar Tepe, (**a**) showing the integration of multisource satellite datasets, interpreted archaeological anomalies, and GNSS stakeout points used for field verification. (**b**) The platform enabled the combined visualization of georeferenced satellite (**c**) layers and (**d**) target points to be replotted in the field, including an offline display mode for on-site navigation, inspection, and ground-truth validation.

The integration of historical and modern satellite datasets allowed the production of thematic maps and cartographic products that provide a holistic view of the site layout, incorporating all previous archaeological interventions carried out at Zar Tepe [10]. These products not only improve macro-scale site interpretation, but also enable the systematic integration of heterogeneous datasets, including multi-source satellite imagery, UAV-derived data, geomagnetic survey results, and evidence from previous archaeological interventions. This data fusion framework supports the delineation of high-probability zones for the presence of buried archaeological remains. Consequently, the proposed methodology constitutes a robust decision-support tool for archaeological prospection in high-complex contexts, where combining historical and modern datasets provides a unique multitemporal perspective on landscape evolution and site formation processes.

2.4. Fieldwork Campaigns

To address the objectives of the Zar Tepe research project, the study was structured around two consecutive archaeological field campaigns organized within a sequential laboratory–field workflow. These campaigns were intentionally scheduled during different seasonal and phenological conditions to maximize the visibility and interpretability of archaeological features. This seasonal strategy is particularly relevant in arid, saline environments, where summer aridity can enhance contrast-driven soil marks (including salt efflorescence), while winter moisture conditions favor geophysical prospection; similar contrast and salinity-conditioned effects on remote-sensing interpretation have been reported in other archaeological contexts [51,52].

The first field campaign, conducted in June 2024, was based on a laboratory-to-field approach and focused on the application of a multiscale and multitemporal methodology using non-invasive remote sensing techniques. This stage aimed to document both visible and buried archaeological remains within the urban enclosure of Zar Tepe (defensive systems, public and residential buildings, artisanal sectors, etc.), as well as within the surrounding landscape (structures, communication routes, field systems, irrigation channels, enclosures, etc.), as a preliminary step before excavation. Simultaneously, the anomalies identified through preliminary satellite-based analysis were field-checked and topographically staked out, while the 2008 plan published by Zavyalov [10], recording the Soviet-era interventions, was georeferenced and accurately repositioned within the site's current topography.

The second field campaign, carried out in December 2025, followed a field–laboratory–field approach and was specifically designed to reinterpret, refine, and validate the results of the first campaign. This phase took advantage of contrasting phenological and soil moisture conditions and focused on ground verification of previously identified anomalies. Particular emphasis was placed on geomagnetic prospection and systematic field validation, allowing the confirmation, refinement, and spatial characterization of archaeological features detected through satellite-based remote sensing analyses.

2.4.1. Georeferenced Stakeout with GNSS (PPP Mode)

During the June 2024 and December 2025 field campaigns, one of the primary objectives was to locate, validate, and topographically verify all satellite-derived anomalies identified during the previous laboratory phase, using a high-precision navigation system capable of unifying all spatial data within a single coordinate reference framework. Although Uzbekistan operates a national CORS network (UZPOS), a Global Navigation Satellite System based on Precise Point Positioning (GNSS PPP) was selected to avoid potential limitations related to mobile network coverage and real-time connectivity to reference station services.

A Leica GS07 GNSS receiver coupled with a CS20 controller was employed. This system operates independently of local RTK reference station networks and provides high-precision positioning through the SmartLink service, achieving real-time centimeter-level accuracy after an initialization period of approximately 10 min, with a final positional accuracy better than 4 cm (Figure 8).

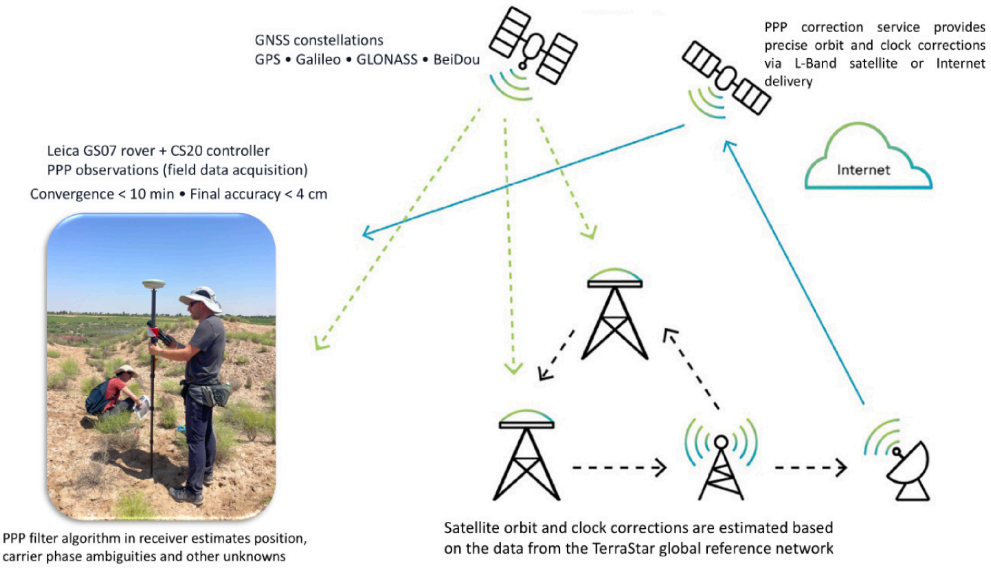


Figure 8. Ground-truthing and topographic verification at Zar Tepe using a Leica GS07 GNSS receiver with CS20 controller in PPP mode (SmartLink), providing centimeter-level positioning (final accuracy < 4 cm) to georeference satellite-derived anomalies, survey grids, excavation areas, terrestrial photogrammetry and UAV ground-control targets within WGS 84/UTM zone 42N (EPSG:32642) during the June 2024 and December 2025 field campaigns.

The GNSS PPP system constituted the spatial backbone of the project, ensuring the integration and spatial coherence of all analyzed datasets, including multisource satellite imagery (CORONA and WorldView-3), UAV-derived photogrammetric products, geomagnetic prospection data, ground-truth verification, the georeferenced 2008 plan published by Zavyalov showing the Soviet-era interventions [10], and archaeological excavation records. Using a single high-precision geodetic framework allowed all observations to be consistently referenced, enabling direct comparison and cross-validation between datasets acquired by different sensors and at different scales. This topographic system was systematically used for staking out and verifying satellite-detected anomalies, establishing survey grids for geomagnetic prospection, spatially locating both the Soviet-era excavation sectors and the newly opened intervention areas and positioning ground control targets for terrestrial and UAV photogrammetry. All spatial data were referenced within the same coordinate reference system (WGS 84/UTM zone 42N, EPSG:32642), ensuring full interoperability between datasets.

The same GNSS PPP methodology was maintained and reused during the December 2025 field campaign, ensuring continuity, spatial consistency, and comparability between both phases of fieldwork, and allowing the progressive refinement and validation of the multiscale and multitemporal analyses conducted at Zar Tepe.

2.4.2. Magnetic Survey

Magnetic prospection was applied in the urban archaeological context of Zar Tepe to detect positive magnetic anomalies resulting from contrasts in the magnetization of buried materials and surrounding soils. The detectability of these anomalies depends on several

factors, including depth, size, magnetic susceptibility, and local background soil conditions. These anomalies are typically associated with anthropogenic features such as ceramic kilns, combustion-related artisanal structures, and domestic hearths. The survey was conducted using a portable, high-sensitivity Geometrics G-864 magnetometer (cesium-vapor type) equipped with two sensors mounted on a rigid rod at a fixed spacing of 0.5 m, allowing rapid and precise identification of subsurface magnetic variations within the fortified enclosure of the site (Figure 9). This dual-sensor configuration enables recording the total magnetic field and results in a gradiometric product from simultaneous measurements (hereafter referred to as magnetometry).



Figure 9. Geomagnetic data acquisition at Zar Tepe (Uzbekistan) using a Geometrics G-864 magnetometer.

During the 2024 campaign, geomagnetic surveys were carried out in four selected areas, including both previously investigated sectors and newly defined zones (P14–P17), following the nomenclature established during the Soviet-period excavations; each area measured 40 × 40 m, except for P15 and P17, which measured 30 × 40 m, with the 30 m side corresponding to the northern edge of the survey area.

Building on the 2024 pilot results, the December 2025 campaign expanded geomagnetic coverage to a systematic grid-based survey of 12 squares measuring 40 × 40 m each (Figure 4), totaling 1.9 ha in the northwestern quadrant of the site, numbered according to the previously established nomenclature and continuing the 2024 designations (from P18 to P29). These grids were systematically arranged in a regular layout of three columns oriented west to east, and four rows, numbered sequentially north–south, ensuring spatial coherence with the 2024 survey areas. This expansion enabled a more continuous characterization of subsurface patterns and provided a broader geophysical context for interpreting productive, domestic, and circulation-related features across adjacent grids and additional data on the urban layout.

The selection of the surveyed areas was based on prior archaeological knowledge of the site and anomalies identified through multiscale remote sensing analysis. Magnetic measurements were collected along parallel profiles within regular grids, with dense sampling intervals allowing interpolation to a final spatial resolution of 0.25 × 0.25 m. Data processing followed standard procedures, including zero-mean grid correction, destaggering, interpolation, and normalization, in order to remove noise and enhance anomaly visibility. The resulting magnetic maps were analyzed to identify linear, sub-rectangular, and point-like anomaly patterns indicative of urban infrastructure and activity zones.

To validate the geophysical interpretation, in situ magnetic susceptibility measurements were taken on selected anomalies using a portable susceptibility meter. Measurements were collected from natural sediments, cleaned cultural layers, and thermally altered materials, enabling the assessment of magnetic contrasts related to anthropogenic activity, particularly high-temperature structures such as pottery kilns.

Targeted surface inspection and limited archaeological excavation were conducted in areas selected based on remote sensing and geomagnetic results to verify the nature of the detected anomalies and refine their interpretation. All spatial, geophysical, and

archaeological datasets were integrated into a georeferenced relational GIS database, which provides the framework for spatial analysis, interpretation, and future excavation planning.

2.4.3. Aerial and Terrestrial Photogrammetry

Aerial photogrammetric documentation of the site was carried out using a combined acquisition strategy based on UAV imagery collected with a DJI Mavic 3 Classic drone equipped with an RGB camera Hasselblad L2D-20c (Hasselblad, Göteborg (Sweden)) (Figure 10), complemented by close-range image acquisition using a Sony A6000 mounted on a 7 m telescopic pole in areas requiring detailed archaeological verification (Figure 11), specifically sectors P14 (2024), P16 (2025), and P20 (2025).

Table 4. Summary of the three UAV photogrammetric flights conducted in June 2024, including acquisition timing, flight altitude, ground sampling distance (GSD), image count, mapped area, and GCP-based georeferencing accuracy (RMSE in XY/Z).

Flight ID	Date	Time of Acquisition	Mean Flight Altitude (m)	GSD (cm/pixel)	Number of Images	Coverage Area (km^2)	No. GCPs—RMSE (XY/Z cm)
1	12 June 2024	Midday (11:34–11:54)	74.2	1.88	291	0.423	15–4.5/4.7
2	12 June 2024	Afternoon (~19:00–20:00)	38.6	1.04	641	0.281	15–4.1/4.1
3	13 June 2024	Morning (09:26–09:32)	46.8	1.21	1110	0.359	15–3.3/2.3

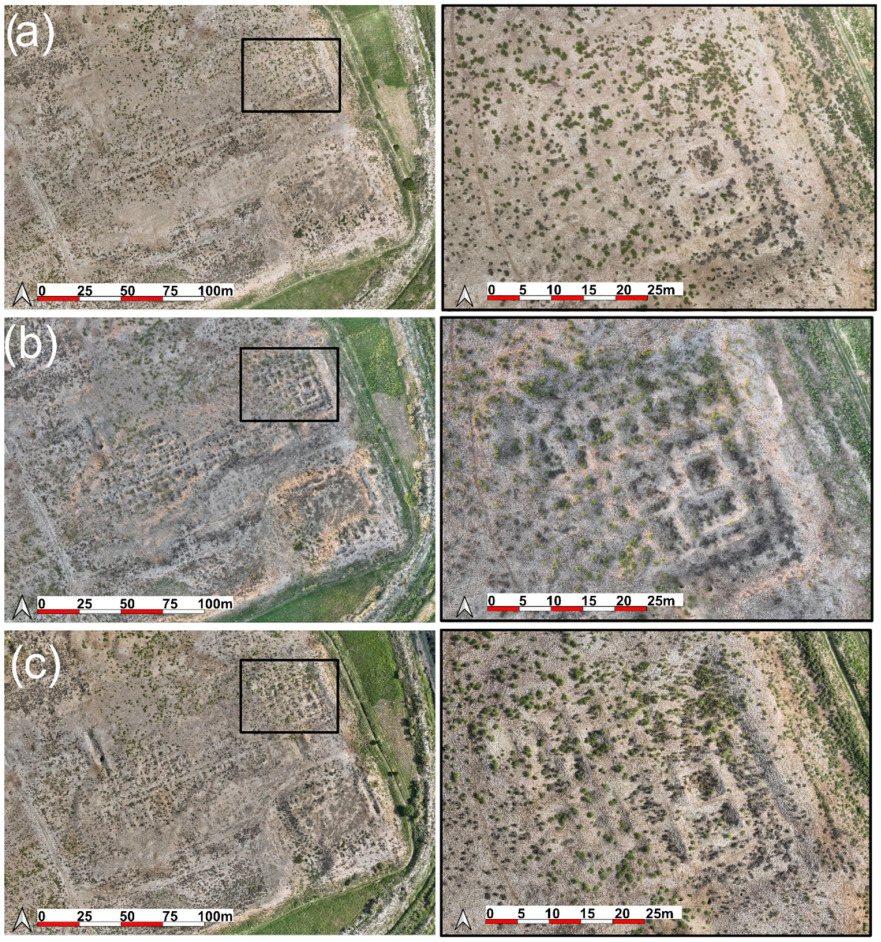


Figure 10. UAV orthomosaics acquired over sector P6 on the same day under contrasting illumination conditions, midday (flight 1, (**a**)), afternoon (flight 2, (**b**)), morning (flight 3, (**c**)) (Table 4), showing the strong influence of sun angle on the visibility of subtle microrelief.



Figure 11. Pole-based terrestrial photogrammetry conducted after the archaeological test excavation in area P14a (sector P14), capturing ultra-high-resolution imagery (target GSD of ~1 mm/pixel) for detailed 3D reconstruction and microtopographic assessment. Red points indicate the vertices of the previously identified geophysical anomaly (Figure 12), used as geospatial control references comparable to GCPs in the photogrammetric documentation workflow.

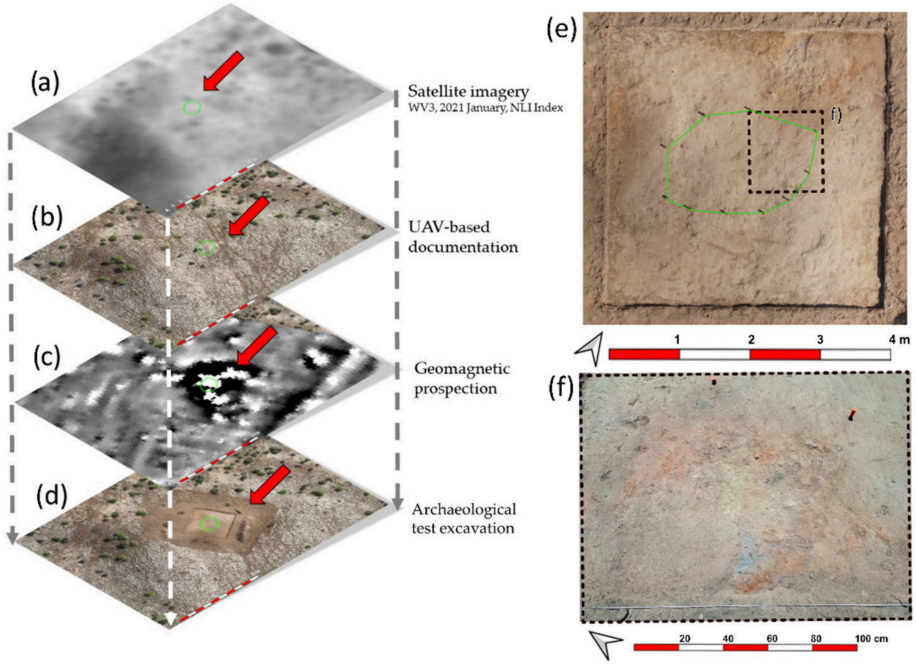


Figure 12. Integrated satellite-to-ground workflow applied at Zar Tepe: (**a**) WorldView-3 satellite imagery, January 2021, NLI index; (**b**) UAV-based documentation; (**c**) geomagnetic prospection; and (**d**) targeted archaeological test excavation in sector P14a. The sequence shows how satellite imagery supported the initial detection of potential archaeological anomalies at the site scale, UAV imagery refined their spatial definition at higher resolution, magnetometry confirmed their subsurface expression and improved their functional interpretation, and excavation provided ground-truth validation. Together, these datasets constitute a multiscale and multitemporal evidence chain for identifying, prioritizing, and verifying buried archaeological structures. (**e**) Orthophotograph of the 4 × 4 m test pit in sector P14a at the end of the shallow verification excavation, June 2024; (**f**) detail of the exposed surface remains of a pottery kiln, with vitrified brick, ashes, and burnt earth visible.

UAV data acquisition was conducted over several days, at different times of the day (morning, midday and afternoon) and at varying flight altitudes in order to evaluate the effect of varying illumination angles on the visibility and interpretation of archaeologi-

cal features. Thus, while the morning dataset provides more homogeneous radiometry, the lower, more oblique afternoon illumination enhances shadowing and tonal contrast, markedly improving the detection and delineation of slight topographic irregularities and surface expressions associated with buried archaeological features (Figure 10).

During the June 2024 UAV survey, the first three flights were conducted under complementary illumination conditions to optimize both geometric consistency and archaeological visibility (Table 4). Flight 1 (12 June, 11:34–11:54) was flown at a mean altitude of ~75 m under balanced illumination, providing radiometrically stable imagery suitable for general mapping and planimetric continuity. Flight 2 (12 June, ~19:00–20:00) was flown at a mean altitude of ~38 m under stronger afternoon light, increasing tonal contrast in bare soil and enhancing subtle archaeological feature detection. Flight 3 (13 June, 09:26–09:32) was flown at a mean altitude of ~45 m and benefited from homogeneous morning illumination, improving spatial coherence within the whole enclosure and supporting consistent site-scale interpretation. Photogrammetric data were georeferenced using 15 ground control points (GCPs) established in situ, consisting of 10 survey targets and 5 field markers, and distributed across the entire site. Image processing was performed using Agisoft Metashape (v2.1.1), generating high-resolution dense point clouds. These datasets were subsequently integrated into the DiGHER web-based platform for further analyses, including elevation assessment, cross-sections, and the generation of Digital Terrain Models (DTMs).

2.4.4. Archaeological Test Excavation

Archaeological verification was carried out through targeted shallow test excavation specifically designed to assess the nature of anomalies detected by the geomagnetic survey and multisource analysis (satellite remote sensing and UAV data) (Figure 12). During the 2024 campaign, two selective interventions were undertaken in sector P14: the first (P14a), measuring 4 × 4 m, was opened in the northern corner, directly along the boundary with sector P15; the second (P14b), measuring 8 × 4 m, was opened in the southwestern corner. Both interventions were recorded using a stratigraphic excavation system. Topographic control and geometric documentation were carried out using GNSS in PPP mode, ensuring all observations were referenced within a single coordinate framework and could be integrated with the remaining project layers (Figure 8). Documentation was complemented with high-resolution digital photographs acquired using a pole-mounted system and processed through photogrammetric techniques to generate detailed plans and metric products, which were subsequently aligned with the remaining datasets.

In 2025, verification was expanded through a cross-validation approach integrating satellite information, UAV-derived products acquired in 2024, and areas prioritized based on magnetometer-detected anomalies. For this purpose, a shallow test excavation was opened in sector P16 by means of one test pit, and two additional test pits were excavated in sector P20 (a and b). These interventions aimed to assess the archaeological nature of the geophysical signatures and refine the functional interpretation of the identified features, including potential productive areas and associated structures.

3. Results

The results are presented following the same sequence as the methodological workflow described above, in order to clarify the specific contribution of each dataset to the archaeological interpretation of Zar Tepe. First, satellite and UAV remote-sensing products are discussed in relation to the detection of surface and subsurface anomalies. Second, geomagnetic prospection results are presented as independent subsurface evidence for architectural and combustion-related features. Third, targeted ground-truth verification is used to assess the archaeological nature of selected anomalies. Finally, all results are inte-

grated within the geospatial database and DiGHER platform to support cross-validation and interpretation.

3.1. Remote Sensing Satellite and Geomatics

Remote-sensing analysis refined the interpretation of Zar Tepe's urban layout by integrating complementary data sources and observation scales. Declassified historical imagery (CORONA/HEXAGON), recent very-high-resolution satellite data (WV3), and UAV-derived photogrammetric products were combined within a coherent multiscale framework. This strategy enabled the identification, mapping, and preliminary verification of numerous architectural traces and spatial patterns throughout the settlement, resulting in a detailed topographic model of the site (Figure 13). The model was generated through non-invasive approaches, including multitemporal remote sensing, UAV-based survey, geophysical prospection, and targeted ground verification. In addition, the multitemporal perspective—based on imagery acquired in different years and seasons—helped discriminate persistent archaeological signatures from transient surface effects, such as phenological vegetation variability and short-lived moisture-related contrasts.

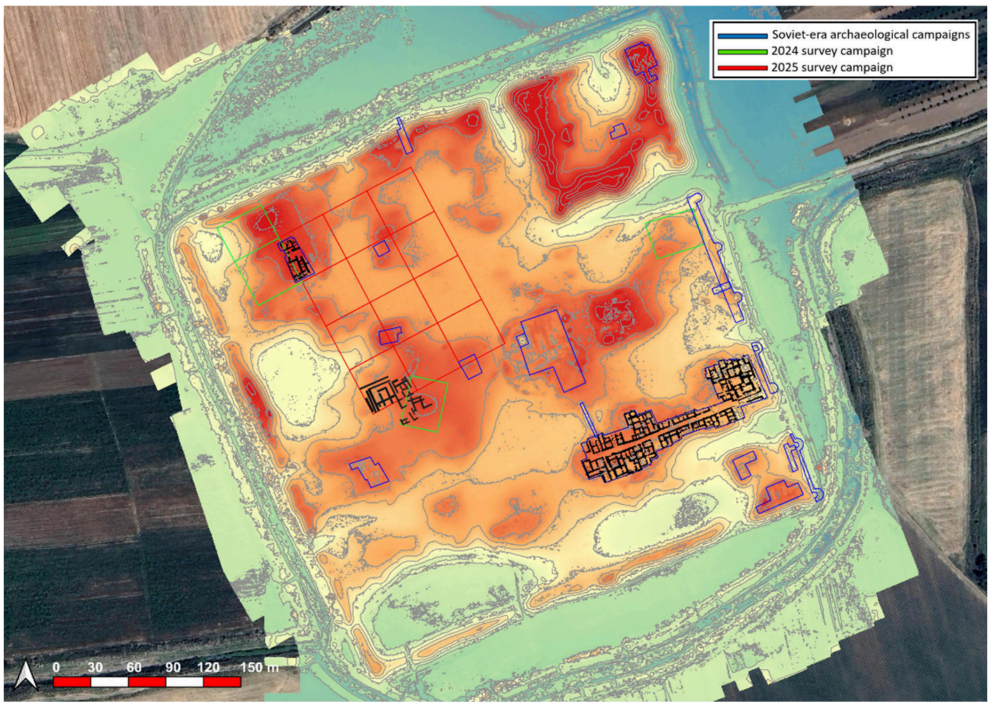


Figure 13. Digital Terrain Model (DTM) of Zar Tepe generated from dense aerial photogrammetric point cloud, georeferenced using GNSS-PPP sensor data, representing ellipsoidal elevations ranging from 262.65 m (blue) to 272.99 m (red).

The results highlight the strong synergy between historical and modern satellite imagery. CORONA images enabled the reconstruction of landscape evolution over the past six decades, revealing changes in vegetation cover and terrain morphology attributable to both human activities and natural processes, while also preserving the visibility of traces related to earlier archaeological interventions that are less legible in the modern terrain. In contrast, WorldView-3 imagery, owing to its high spatial resolution and the application of radiometric correction and data fusion techniques, enabled the detection of fine-scale features, such as the settlement's internal street network, small remnants of defensive structures, and the surface expression of previously excavated areas, which are not always discernible in historical satellite data.

The research conducted has led to the identification of many structures belonging to the site's urban grid, spanning both the citadel area and the entire walled settlement. Processed satellite imagery of the northwestern quadrant of Zar Tepe using vegetation/soil indices and Principal Component Analysis (PCA) revealed numerous anomalies that were topographically staked out in the field using a GNSS workflow operating in PPP mode, supporting target selection for subsequent geophysical survey and archaeological ground-truth verification. The analysis clearly revealed spatially coherent linear and block-like patterns consistent with an orthogonal urban layout and activity-related zones, as demonstrated by the alignments of major access routes and streets of varying hierarchy connecting the known gate locations along the perimeter wall. Some of these roads linked Zar Tepe with other contemporary sites in the region, such as ancient Termez to the south, Kampir Tepe to the west, and Dalverzin Tepe and the upper Surkhandarya Valley to the northeast. The imagery further suggests the layout of possible residential quarters, distinctive buildings, and open areas within the site, which will require systematic stratigraphic excavations to confirm their functions.

Drone flights conducted at different times of day—hence capturing different shadow orientations (Figure 10)—revealed subtle surface undulations and alignments, corroborating the street grid and building locations hypothesized from the older maps. The integration of drone-derived imagery with satellite and cartographic data further enhanced the definition of urban structures at Zar Tepe. In particular, the DTM accentuates subtle topographic variations and highlights the outlines of archaeological features, including former excavation areas and building remains (Figure 14a,c). When combined with georeferenced historical plans, multi-period satellite images, and CORONA/WV3-derived information, these drone datasets enabled the creation of detailed 3D models of the site using photogrammetric Structure from Motion (SfM) techniques. Together, these three-dimensional reconstructions and the multitemporal analysis of satellite and UAV imagery provided the basis for a substantial revision of the Zar Tepe site plan. We produced an up-to-date composite plan that synthesizes all available evidence of the site's morphology to serve as a robust basis for guiding current and future investigations. This integrative approach also enabled a more accurate spatial fitting of the Soviet-era interventions documented by Zavyalov [10], drawing on both high-resolution photogrammetry and, in particular, the DTM derived from the UAV dense point cloud. The DTM, referenced to consistent elevation values, enhances the detection of subtle microrelief and, therefore, improves the spatial alignment of the previously excavated sectors (Figure 13). Notably, several areas partially excavated in the 1970s are discernible as depressions or patches in the modern DTM (Figure 14), including Soviet excavation trenches like sectors P1, P6, P8, and P9. In addition, the images reveal structures corresponding to previously documented buildings both inside the fortified enclosure [10] (e.g., sectors P1, P3, P5–8, P11, P12) and in the citadel (sectors P10, P13), as indicated on previous plans. This refinement is essential to correct earlier topographic positioning, integrate newly identified features in previously undocumented areas, and interpret the urban layout with greater reliability, further supported by on-site stakeout and verification using a GNSS workflow operating in PPP mode (e.g., sector P8, Figure 14).

In addition to cropmarks and shadow-related anomalies, a second type of soil mark, associated with salt efflorescence processes, was documented during the June 2024 field campaign through UAV imagery. This field campaign at Zar Tepe yielded particularly favorable results for detecting buried archaeological structures through UAV-based documentation, largely due to the presence of salt efflorescence acting as a surface indicator in this arid environment. The site's environmental conditions—located on the alluvial plain of the Surkhandarya valley, characterized by saline soils, a markedly continental climate,

and extreme summer temperatures exceeding 40 °C—are especially conducive to capillary rise and evaporation processes.

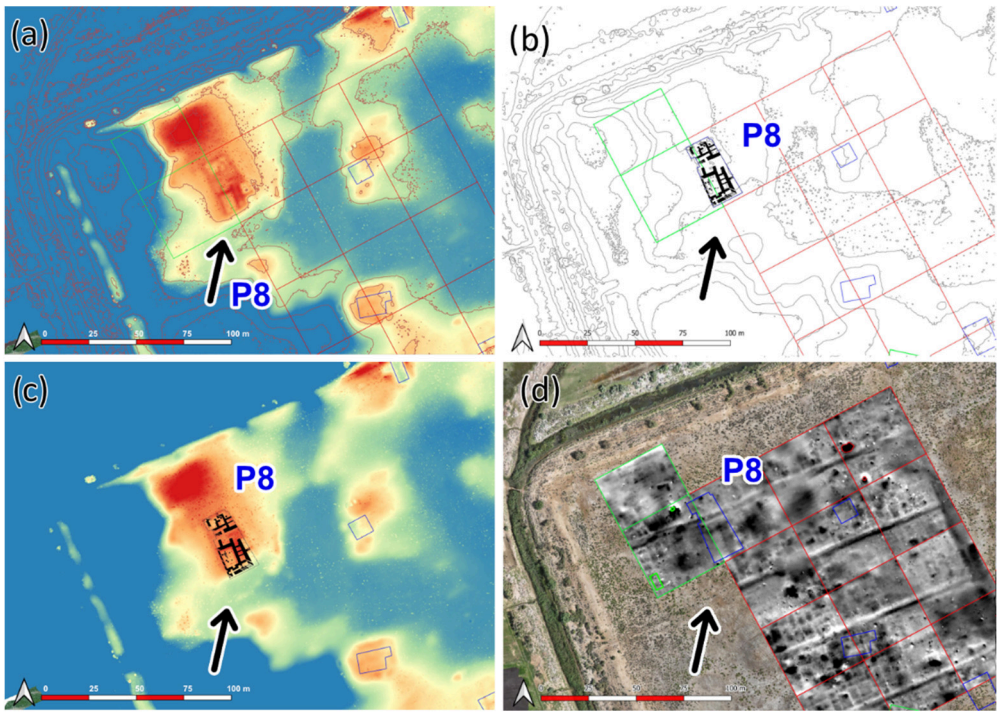


Figure 14. Spatial fitting of sector P8 based on microtopographic, geodetic, and geophysical evidence. (**a**) Photogrammetry-derived DTM showing the broader relief anomaly associated with P8, indicated by the arrow; the model was georeferenced and refined using GNSS Precise Point Positioning (PPP), with ellipsoidal heights ranging from 270.24 m (blue) to 272.99 m (red). (**b**) Contour-based visualization showing the correspondence between the preserved microrelief and the digitized plan of P8. (**c**) Detailed DTM view illustrating the fit between the archaeological plan and the local topographic anomaly. (**d**) Integration with geophysical survey data and the current orthophotographic background, showing the relationship between P8, the survey grid established in 2024 (green squares) and 2025 (red squares), and subsurface anomalies.

Whitish linear anomalies, visible in both UAV imagery acquired during the June 2024 campaign and WorldView-3 data, spatially coincide with buried walls of previously undocumented urban structures that had not been recorded in the Soviet-era excavations before 1986 (Figure 15). The spatial recurrence and geometric consistency of these anomalies, verified through geomagnetic prospection in the December 2025 campaign, strongly support their interpretation as salt efflorescence conditioned by buried archaeological structures rather than random edaphic variations. In contrast, winter conditions in the December 2025 field campaign, with lower temperatures and higher soil moisture, inhibited evaporation processes, effectively suppressing the formation of salt efflorescences. Although the phenomenon was absent under winter conditions, magnetic prospection carried out at that time reinforced the documentation of the same subsurface urban features previously detected by UAV imagery.

From a remote-sensing perspective, salt efflorescences associated with buried archaeological structures are characterized by localized increases in spectral reflectance, well-defined radiometric contrasts relative to the surrounding soil, and enhanced detectability under conditions of maximum insolation, extreme thermal stress, and surface dryness. These anomalies can be identified in both UAV-based very-high-resolution imagery and satellite data, with their interpretation further strengthened through multitemporal analysis, principal component analysis, and the application of soil-oriented spectral indices.

In this context, salt-efflorescence soil marks constitute a valuable non-invasive proxy for detecting buried urban features at Zar Tepe, enabling the identification and delineation of architectural remains even in the absence of surface relief or vegetation when corroborated by independent datasets. Their integration into a multiscale, multitemporal and multi-illumination remote-sensing framework significantly enhances archaeological documentation and interpretation strategies in arid landscapes.

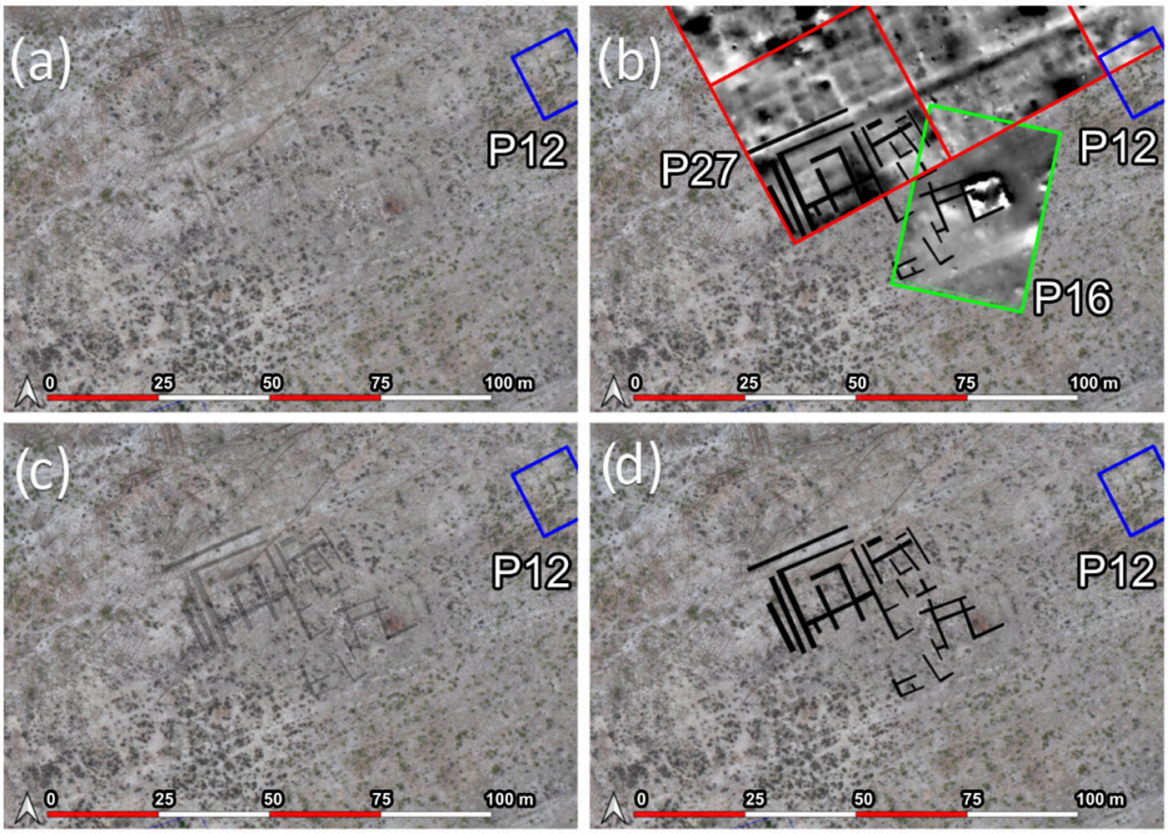


Figure 15. (**a**) UAV orthomosaic (June 2024) showing whitish high-reflectance linear anomalies produced by salt efflorescence above buried architectural remains in sectors P16 and P27–P28 at Zar Tepe. In the saline alluvial setting of the Surkhandarya valley, extreme summer temperatures and low humidity intensify capillary rise and evaporation, concentrating soluble salts and generating surface efflorescences that preferentially develop over subsurface walls (capillary-barrier effect). (**b**) Geomagnetic prospection results in sector P16 (June 2024, green highlighted area) and sectors P27–P28 (December 2025, red highlighted area), confirming the same subsurface architectural layout, and supporting the archaeological origin of the salt-efflorescence soil marks detected in the UAV imagery. (**c**,**d**) Interpretative overlay of the inferred buried architectural remains superimposed on the orthomosaic, displayed with two different transparency levels to facilitate visual comparison between the proposed structural layout and the underlying surface evidence.

3.2. Magnetic Prospecting Techniques

Geomagnetic prospection at Zar Tepe enabled rapid, non-invasive detection of subsurface archaeological features, directly supporting the project's objectives related to (i) reconstructing the settlement's internal layout and (ii) identifying productive/activity areas characterized by combustion-related signatures.

In 2024, magnetometry was applied in four targeted areas (P14, P15, P16 and P17) to test specific hypotheses derived from prior excavation reports and remote-sensing observations. Data were acquired along regular walking transects with constant spacing and speed, following a grid-based layout. During the systematic 2025 campaign, grids

generally measured 40 × 40 m and were surveyed along parallel profiles with a line spacing of 1 m; data were recorded at 20 Hz, producing dense sampling optimized for small-scale archaeological features. All measurements were georeferenced using GNSS to ensure direct spatial integration with satellite imagery, orthophotographs, and excavation maps.

Data processing was performed in Geoplot 4.00 following a standardized workflow including Zero Mean Grid, interpolation along profiles, destaggering to correct zig-zag offsets, interpolation between profiles, and Zero Mean Traverse, with datasets finally merged into a continuous georeferenced map ("Cut and Combine"). Based on the acquisition geometry, the original sampling resolution was 0.25 × 0.50 m, and after interpolation, the final visualization grid reached 0.25 × 0.25 m resolution.

The first survey area was located in the northwestern part of the site and encompassed excavation sectors P14 (40 × 40 m) and P15 (30 × 40 m) (Figures 4 and 14). This zone lies just northwest of sector P8 (excavated in 1977 by S. R. Pidaev), where earlier investigations reported structural elements possibly related to ceramic kilns [10,36]. Therefore, the primary objective was to detect kiln-like magnetic signatures. Results revealed well-defined, high-contrast anomalies strongly suggestive of at least one rectangular firing installation consistent with a ceramic kiln. The geometry and dimensions are comparable to kilns documented at regional Kushan and Kushano–Sasanian centers (e.g., Dalverzin Tepe; ancient Termez) [19,55,56]. These results guided the placement of the first 4 × 4 m test excavation in the northern part of sector P14a, which confirmed the presence of kiln-related remains (Section 3.3).

The second survey area, P16 (40 × 30 m), was positioned in the central portion of the settlement, west of sector P12, an area without previous excavation. In 2025, a targeted shallow test pit was opened within P16 to ground-truth the geophysical anomalies. Remote sensing and UAV observations suggested subsurface features, including potential combustion installations. Magnetometry identified a cluster of anomalies forming a roughly square arrangement, designated P16 (Figure 15). The signatures are compatible with small circular combustion structures associated with the walls of a room or building. While excavation is required to determine their exact function, preliminary interpretations include domestic ovens/hearths, small furnaces/kilns related to artisanal activity, and/or installations with a possible cultic component.

The third survey area, P17 (30 × 40 m), was surveyed south of the citadel, in front of towers 2 and 3 along the eastern stretch of the defensive wall (Figure 4). The aim was to evaluate the ability of magnetometry to detect adobe architecture and domestic activity features in a previously unexplored zone. The results revealed anomalies indicative of habitation-related structures and possible domestic hearths. These interpretations will require stratigraphic verification in future excavation phases.

Magnetometry datasets from both seasons were processed using a standardized pipeline including outlier removal (despiking), line levelling/detrending to minimize striping and low-frequency background variation, and interpolation to a regular grid for visualization and spatial comparison with other layers (remote sensing, UAV products, and archaeological plans). This approach highlighted the main features of the urban layout. All anomalies were precisely georeferenced using GNSS-PPP mode and, where appropriate, physically staked out on the ground to facilitate immediate field verification, as illustrated specifically by the P14a intervention in Figures 11 and 12e, and more generally by the magnetometry survey areas and detected anomalies shown in Figure 16.

Overall, based on the combined analysis of the 2024 and 2025 datasets, and pending further field verification in future campaigns, the 2025 anomaly patterns further supported the preliminary interpretation of: (i) elongated linear anomalies compatible with possible street segments and circulation corridors; (ii) sub-rectangular anomaly blocks consistent

with architectural units aligned with the inferred street grid; and (iii) clusters of high-contrast anomalies suggestive of combustion-related activity areas. Taken together, these results provided broader spatial continuity for features first detected in 2024 and helped define priority areas for subsequent archaeological testing and phased excavation planning (Figure 15).

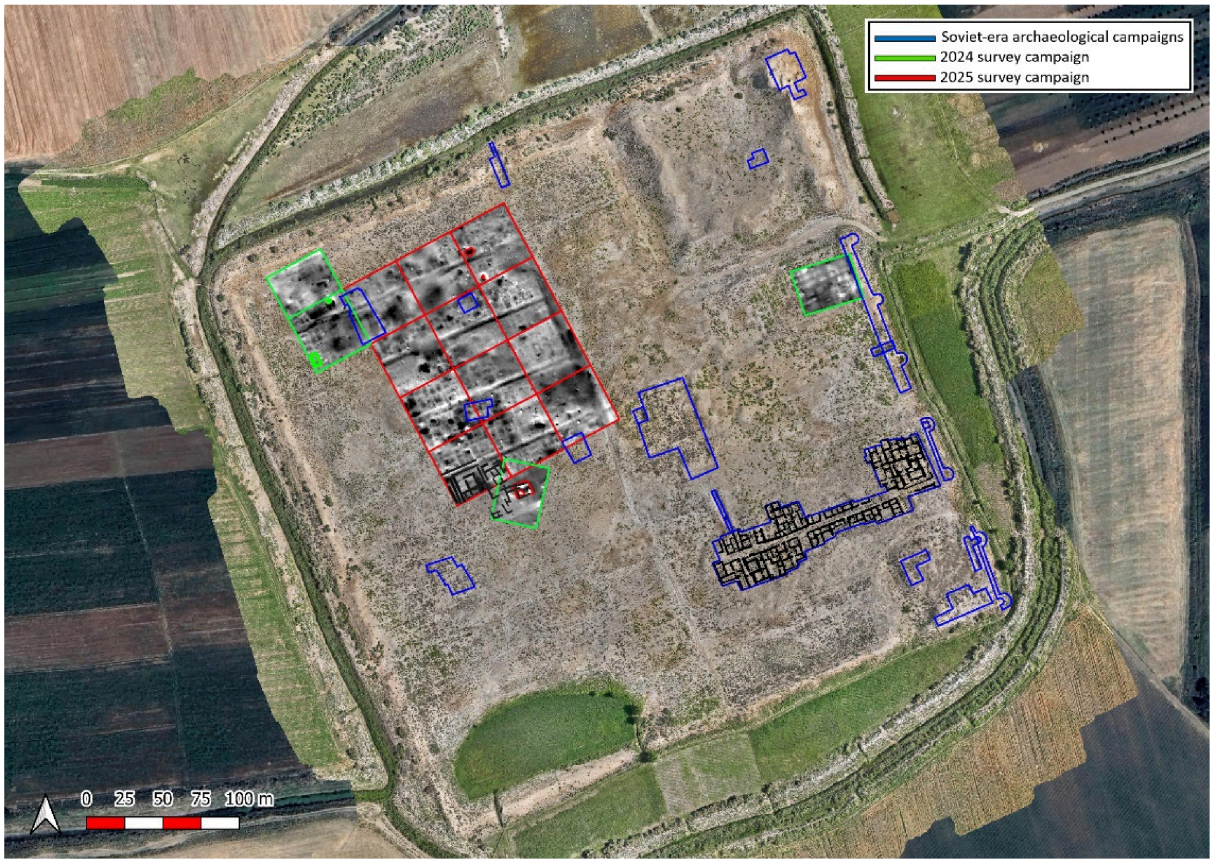


Figure 16. Locations of the areas surveyed with magnetometry results (outlined) superimposed on a WorldView-3 (WV3) satellite image and the high-resolution orthomosaic of Zar Tepe (UAV), with the outlines labeled to indicate their correspondence with the different excavation sectors. The greyscale magnetic map (P14–29) shows values ranging from −12 to +12 nT.

Finally, the integration of magnetometry with remote-sensing overlays and targeted ground checks improved the spatial interpretation of functional zoning at Zar Tepe and established a preliminary interpretation for guiding future stratigraphic excavations.

3.3. Ground Truth Verification: Prospection and Archaeological Excavation

The GNSS PPP mode was crucial during the verification phase, enabling accurate georeferencing and stakeout of all features of interest across the site. With centimeter-level precision, it was possible to relocate on the ground the exact positions of features observed in satellite/UAV imagery or detected through magnetometry, ensuring test pits and trenches were correctly placed. This procedure allowed us to define the full extent of the site's visible archaeological area and generate a detailed topographic plan mapping all documented sectors—both from previous excavations and newly identified in 2024—at their correct locations within the site and the surrounding landscape. All field data (e.g., point coordinates, structural outlines) were continuously integrated into the project GIS together with relevant cartography, satellite imagery, and aerial photographs, ensuring

that newly acquired ground information was immediately incorporated into the overall spatial interpretation of the site.

Geomagnetic surveys conducted in 2024 and 2025 corroborated specific archaeological features identified through georeferenced historical plans, satellite imagery, and UAV data, including wall alignments and possible elements of an urban grid associated with buildings and streets. The archaeological exploration conducted in parallel, which targeted specific magnetometry-detected anomalies in sectors P14, P16, and P20, further reinforced the remote sensing analysis and the geomagnetic survey results. For example, the cluster of anomalies in sector P16 (first identified during the 2024 survey) was staked out and correlated with slight depressions and/or subtle soil color variations, supporting the interpretation of subsurface structures. Subsequently, during the 2025 campaign, a shallow test excavation in P16 corroborated the presence of a feature that may correspond to a kiln-related structure. Overall, excavation-based verification targeted the strong anomaly in sector P14a, one anomaly in sector P16, and two additional anomalies in sector P20, as described below.

During the first field campaign, archaeological excavation was deliberately limited to shallow interventions in two small areas within sector P14. Given the short duration of the 2024 campaign, full stratigraphic excavation of any single area was not feasible. Instead, these interventions were designed as verification test pits aimed at checking specific anomalies or surface indications identified through remote sensing and survey. Accordingly, the excavations functioned as ground-truth checkpoints to validate remote-sensing and magnetometry results, rather than extensive horizontal exposures.

Test pit P14a (4 × 4 m) (Figure 4b), opened in the northern part of sector P14, was placed over the prominent magnetic anomaly detected in survey area 1, in the northwestern part of Zar Tepe. Its location was further supported by very-high-resolution WorldView-3 imagery, including SAVI (May 2017), PCA component 14 (December 2018), and OSAVI (August 2017). After removing the topsoil and very shallow overburden, the excavation immediately revealed evidence of intense burning, including fragments of vitrified adobe bricks, patches of reddened soil, and ash and charcoal remains. These indicators demonstrate in situ high-temperature firing and confirm the presence of at least one ceramic-kiln structure in this area. The remains, including partially sintered mudbrick and burnt deposits, suggest that the kiln walls and/or dome may have collapsed and fused under heat. Figure 12 shows the P14a test pit at the end of the shallow excavation, together with a close-up of the exposed kiln remains. This discovery provides direct evidence of pottery production at Zar Tepe and validates the hypothesis—based on satellite observations, magnetometry, and indications from the 1970s excavations—that a pottery workshop operated in this part of the settlement.

A second trench, P14b (8 × 4 m), was opened in the southwestern part of sector P14, in an adjacent area south of P14a, to investigate a space that, according to satellite data, magnetometry, and surface survey, might contain remains associated with the kiln area, such as workspaces or storage facilities. In this shallow excavation, several in situ features were identified almost directly below the surface. Most notably, three large ceramic vessels interpreted as storage jars were found fixed in place at different elevations within the trench. Two jars were fragmentary, whereas one, at slightly greater depth, appeared largely intact with only the rim visible at the surface. These vessels likely represent a storage area, possibly a terraced zone where large containers were set into the ground for storing goods. Their size and clustering suggest a purpose-built storage installation. This arrangement is comparable to storage areas documented in earlier Soviet excavations, for example, in sector P6 (Rooms 120/124 and 159), where large jars were embedded into the floor. The P14 findings therefore point to part of a storage or inventory space, potentially

associated with the adjacent pottery-production area or representing another building used for storage and perhaps distribution. Although only a small portion was uncovered, these finds significantly advance our understanding of economic and functional zoning within the settlement.

During the 2025 field campaign, the initial plan was to continue shallow excavation in sector P16 and to assess in situ the results of the new magnetic prospection survey, carried out using a gridded layout between P19 and P29. Given that this area had been subjected to small-scale interventions during the Soviet period (P8, P5, P3, and partly P12), the aim was to obtain a sufficiently broad overview to evaluate the potential urban layout of this sector and the presence of associated anomalies. Only the Digital Terrain Model (DTM) developed in 2024 allowed the P8 excavation to be located with reasonable precision (Figure 14). The remaining evidence became apparent only after processing the 2024 datasets, thanks to a high-quality orthophoto and the previously discussed salt-efflorescence phenomenon affecting buried structures. Because the area is largely unexcavated, the DTM did not display clear anomalies or diagnostic microrelief features like those seen in P8 (Figure 14). In this context, magnetic prospection enabled the detailed identification of a highly regular urban structure, consistent with salt-efflorescence indicators detected after processing the 2024 campaign data, but only within the P27–P28 area (Figure 15).

Accordingly, the anomaly previously identified in P16 during the 2024 survey was tested through a shallow excavation measuring 9 × 8 m, which exposed a combustion-related structure in its central sector, tentatively interpreted as kiln-related. In addition, two anomalies detected by magnetic prospection in sector P20 were partially excavated; these were aligned with the previously identified urban grid and served as additional verification points for the integrated interpretation of this part of the site.

Due to the limited scope of the verification test excavations in sector P20, deeper stratigraphic layers beyond the uppermost occupation and/or destruction deposits were not reached, and the amount of recovered material was not sufficient for broader analyses.

More generally, although the archaeological interventions conducted in 2024 and 2025 followed a stratigraphic excavation approach, their limited depth and extent did not allow for the documentation of well-developed stratified sequences or the recovery of datable organic material (e.g., for radiocarbon dating). These objectives are therefore deferred to future excavation seasons, when larger areas can be opened and systematically excavated.

3.4. Geospatial Data Integration, Web Mapping, and 3D Point-Cloud Management

All spatial and archaeological information generated during the project was integrated into a relational GIS geodatabase, including historical Soviet-era plans, updated archaeological interpretations, satellite-derived anomalies, UAV orthomosaics and DTMs, magnetometry grids, GNSS-PPP records, excavation sectors, and ground-truth observations. This common spatial framework allowed direct comparison between datasets acquired at different scales and resolutions, supporting the cross-validation of remote-sensing, geophysical, and archaeological evidence.

The geodatabase was implemented in the DiGHER web platform developed at the University of Zaragoza, providing an interactive 2D/3D environment for data visualization, field planning, and interpretation. The platform enables users to overlay historical imagery, WorldView-3 products, UAV-derived models, magnetometry results, and excavation data; to inspect feature attributes; and to generate annotations, measurements, profiles, and cross-sections (Figure 17). In operational terms, the platform supported the iterative workflow of the project by linking satellite- and UAV-detected anomalies with GNSS-PPP stakeout, geomagnetic prospection, and targeted archaeological verification.

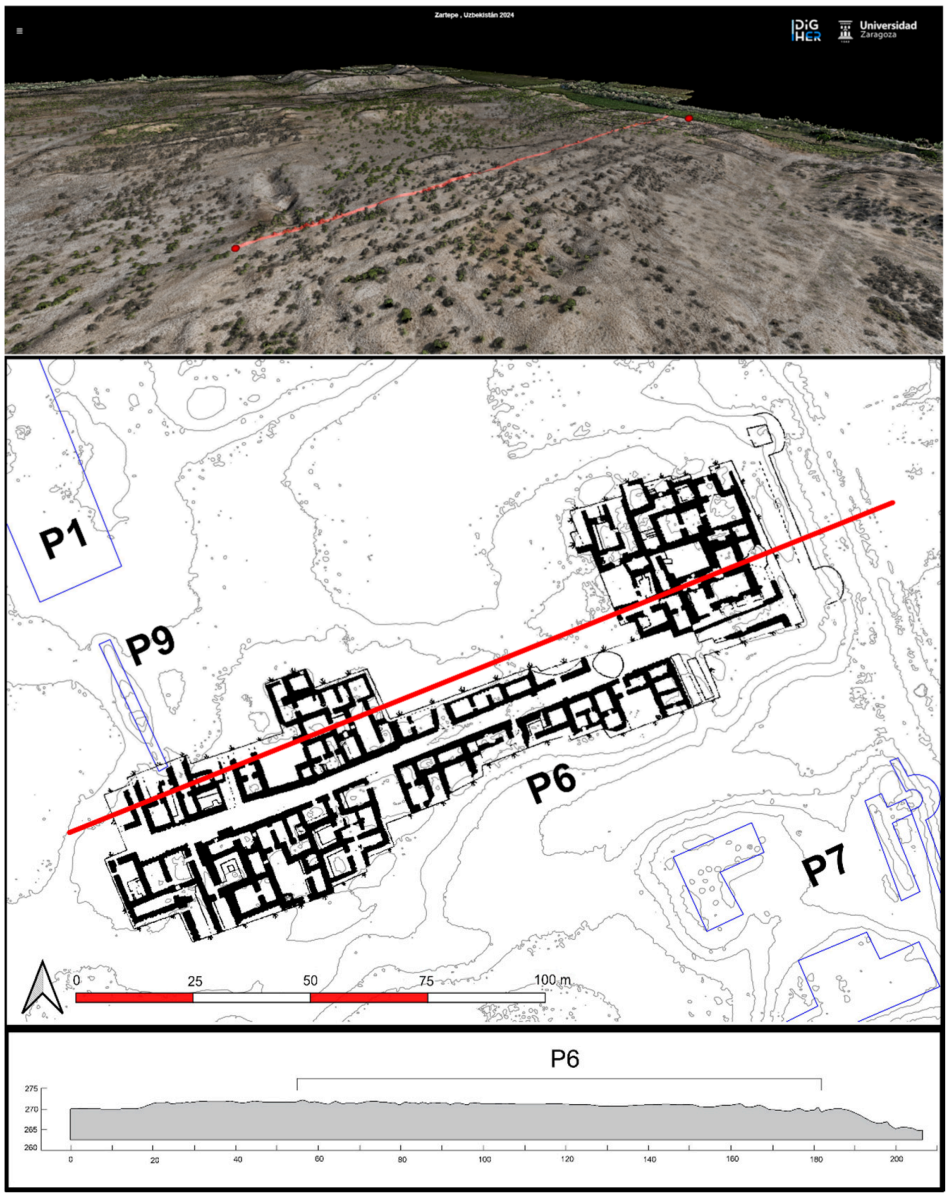


Figure 17. Schematic representation of the point-cloud integration workflow in the DiGHER platform (top). Point-cloud files in E57, LAZ, and LAS formats are processed, standardized, and aligned server-side, and then delivered through an interactive WebGL-based viewer that supports on-demand measurements and semantic enrichment. The workflow also enables the extraction and export of geometric products directly from 3D data—such as profiles and cross-sections—for quantitative assessment; an example from an exported section/profile (P6 sector) illustrates in-platform slicing of the point cloud for feature inspection and field cross-checking.

In addition to its role as a visualization tool, DiGHER functions as a structured digital repository for the progressive construction of a site-scale archaeological digital twin. Each 2D and 3D asset is linked to its acquisition and processing context, improving traceability, provenance control, and the reproducibility of interpretations across successive field seasons.

4. Discussion

The Uzbek–Spanish archaeological project at Zar Tepe marked the resumption of research at the site after a long hiatus following the Soviet-era excavations. Over two complementary field seasons (June 2024 and December 2025), the combination of remote sensing,

geomatic surveying, geophysical prospection, and targeted test pit excavations addressed the project's main objectives and yielded significant new insights. At the macro scale, the integrated, non-invasive workflow produced an improved graphic and cartographic record of the site, enabling a more refined assessment of Zar Tepe's urban morphology and its relationship with the surrounding landscape. At the micro- and meso-scale, the detection and verification of archaeological features in multiple sectors (P14, P16, P20, P27 and P28), particularly those linked to combustion installations and productive or artisanal activities, together with the identification of a highly regular urban architectural layout confirmed by both optical and geomagnetic evidence, as well as elements attributable to later occupation phases, provide a more robust basis for interpreting the site's internal functional organization. While the results are still preliminary, they are consistent across datasets and highly promising for continued research.

The multiscale and multitemporal remote-sensing approach proved especially effective. By combining georeferenced historical plans, multi-date satellite imagery with varying spatial and spectral resolutions, and very-high-resolution UAV products, we detected numerous structures associated with the settlement's street grid and building blocks, especially within the walled enclosure. In parallel, the production of an updated Digital Terrain Model and UAV-based 3D reconstructions (SfM) provided a nuanced perspective on subtle topographic expression, preservation state, and the legibility of previously excavated areas. Importantly, the seasonal strategy strengthened interpretative reliability: summer conditions favored the expression of high-reflectance soil marks (including salt-related efflorescence) that outlined buried architectural features, while winter conditions reduced optical contrasts but enabled systematic geophysical mapping and broader on-site verification under more favorable moisture conditions. These contrast-driven visibility effects, likely intensified by salinity-related surface processes, have been discussed in multispectral approaches to archaeological detection, where subtle spectral contrasts and environmentally conditioned signals can both support and bias interpretation [51,52]. At Zar Tepe, the correspondence between salt-efflorescence soil marks and coherent geomagnetic anomalies reduces interpretative uncertainty and supports an architectural origin for the mapped patterns. This relationship is particularly relevant in the saline alluvial setting of the Surkhandarya valley, where soluble salts may accumulate through alluvial processes, long-term irrigation practices, and prolonged evaporation cycles.

During summer, high temperatures and low relative humidity can activate a combined process of upward capillary water movement and rapid surface evaporation. As groundwater rises through soil pores, dissolved salts are brought to the surface, where evaporation causes their precipitation and crystallization as visible surface crusts.

The resulting surface deposits significantly alter the soil's radiometric properties, increasing surface reflectance in the visible range and producing light-toned or whitish anomalies [51,52]. Such features are clearly detectable in very-high-resolution UAV imagery. In archaeological contexts such as Zar Tepe, the interaction between salt-efflorescence processes and buried earthen structures may amplify this contrast. Subsurface walls constructed of adobe, rammed earth, or stabilized earthen materials can modify local soil porosity and permeability, promote differential moisture retention, and interrupt vertical water flow by acting as capillary barriers. Consequently, capillary rise and salt crystallization may intensify preferentially above buried walls, generating linear or geometric high-reflectance anomalies that reproduce the layout of subsurface architectural features. These anomalies appear as soil marks and are particularly effective indicators in environments with minimal or absent vegetation cover.

A GNSS-based workflow operating in Precise Point Positioning (PPP) mode served as the geodetic backbone of the project during both campaigns, providing substantial

logistical flexibility while maintaining a single, consistent spatial reference framework. It enabled centimeter-level relocation and stakeout of features identified in maps, satellite/UAV imagery, and magnetometry, ensuring that verification observations, geophysical grids, and excavation test pits were positioned accurately and could be directly compared. This unified coordinate framework (EPSG:32642) substantially supports the ongoing updating and reinterpretation of the Zar Tepe site plan and provides a stable spatial basis for future excavation strategies, monitoring, and inter-site comparison within Bactria and the surrounding regions.

Geomagnetic prospection proved to be a particularly efficient tool for detecting subsurface architectural patterns and combustion-related features, rapidly supporting objectives focused on urban layout reconstruction and the identification of productive areas. The 2024 magnetometry provided an initial assessment in several discrete, spatially separated areas (P14–17), while the 2025 campaign substantially expanded coverage with a systematic grid-based design (P18–29). This allowed for the evaluation of anomaly continuity and spatial patterning over a larger portion of the northwestern sector. The magnetic datasets reveal both linear and block-like signatures consistent with adobe-built structures and street alignments, as well as clusters of high-amplitude anomalies most plausibly linked to burning installations and activity areas. This 2025 expansion moved the study beyond isolated observations, enabling the identification of recurrent anomaly types and their distribution relative to the urban grid.

The targeted test excavations undertaken in 2024 and 2025 provide key ground-truth anchors for these non-invasive interpretations. In 2024, the integration of magnetometry with shallow excavation in P14a proved especially productive, confirming the presence of at least one pottery kiln, as indicated by vitrified adobe, reddened soils, and combustion residues. These findings directly validate the interpretation of strong magnetic anomalies as firing structures and support the hypothesis, suggested by both earlier Soviet observations and recent remote-sensing evidence, that craft production was integrated into the settlement's spatial organization.

Shallow excavation in P14b identified large storage jars set in place, closely paralleling storage installations described in earlier Soviet excavations (e.g., sector P6) [10]. Although only a small area was exposed, the association of storage features with the kiln zone in sector P14 strengthens the interpretation of the northwestern quarter as an integrated production–storage area. This location—close to a principal gate and aligned with the internal street network—would be a logical setting for craft activities, storage, and potentially the distribution both within the city and to neighboring centers. In this sense, the P14 results offer the first empirically supported insight into functional zoning at Zar Tepe. The 2025 season added an essential second layer of verification by extending the assessment to additional sectors and undertaking shallow excavation in areas prioritized by geophysical and remote-sensing indicators. In sector P16, surface observations and magnetometry-guided interpretation were followed by a shallow intervention that corroborated a feature compatible with a firing installation, reinforcing the broader pattern of combustion-related activity in the northwestern zone. Additional test pits in sector P20 provided further cross-checks between satellite/UAV observations and geophysical signatures, contributing to a more spatially distributed set of validation points. Collectively, these 2025 interventions reduce interpretative uncertainty by demonstrating that high-amplitude magnetic anomalies correspond to meaningful anthropogenic features rather than random edaphic variation. Beyond productive areas, the combined datasets also suggest the presence of previously undocumented urban elements. Magnetometry and remote-sensing overlays indicate coherent linear features compatible with circulation corridors and a more extensive, probably orthogonal architectural grid than that captured in the Soviet-era excavation

footprint. These findings are consistent with the interpretation of Zar Tepe as a complex urban settlement that may have included differentiated spaces for habitation, production, storage, religious practice, and defense, although the nature, chronology, and extent of these functional areas require confirmation through future stratigraphic excavation. Future work in P14 and P16 should clarify the number and layout of kilns, establish a more secure chronology, and recover diagnostic assemblages for comparison with ceramic production evidence from nearby centers such as Termez and Dalverzin Tepe.

In summary, the investigations conducted to date have substantially enhanced the archaeological understanding of Zar Tepe by providing an updated, cross-validated interpretation of its spatial organization. The key contribution of the 2024–2025 project phase is both methodological and archaeological: the seasonal, multi-sensor strategy demonstrates that the main anomaly patterns are consistently recognizable across independent optical and geophysical datasets and under different acquisition conditions. However, it must be emphasized that the present excavations were intentionally limited in depth and extent; thus, while they confirm certain feature types and support functional interpretations, they do not yet provide a full stratigraphic sequence or robust dating framework. The next steps should therefore include expanded stratigraphic excavation in selected priority areas, systematic sampling for absolute dating where feasible, and the recovery of larger artefact and bioarchaeological assemblages to address chronology, economy, and resource exploitation between the 1st and 5th centuries AD. Such data will enable more robust comparisons with other Bactrian urban centers and contribute to broader discussions of Kushan-period urbanism and cultural landscapes in Central Asia.

5. Conclusions

The two-field-season Uzbek–Spanish investigations at Zar Tepe (June 2024 and December 2025) demonstrated the effectiveness of an integrated satellite-to-ground workflow combining multitemporal remote sensing, GNSS-PPP control, geomagnetic prospection, UAV photogrammetry, and targeted archaeological testing. By combining satellite and UAV observations with GNSS-PPP geodetic control, magnetometry, and shallow verification excavations, the project substantially updated and expanded the available knowledge of Zar Tepe beyond the legacy of Soviet-era research.

The results support the hypothesis of a broadly regular, probably orthogonal urban layout, revealed through convergent optical and geophysical evidence. Specialized activity areas were also identified, including one excavated kiln-related installation and possible storage features. Together, these findings provide new evidence consistent with the role of Zar Tepe as a settlement where pottery production and storage activities formed part of the urban organization, although their full extent and chronology require further stratigraphic excavation.

A major contribution of this study is methodological. The project design explicitly leveraged seasonal contrast to improve interpretative confidence in an arid, saline alluvial environment. Summer conditions (June 2024) enhanced the optical expression of buried architecture, particularly through high-reflectance soil marks related to salt efflorescence, whereas winter conditions (December 2025) reduced optical contrasts but provided favorable conditions for systematic geophysical mapping and broader on-site verification. The convergence of independent observation modalities across two seasons strengthens the reliability of the detected anomalies and reduces the likelihood that the interpreted features are tied to a single acquisition window or short-lived surface phenomena.

The 2025 campaign marked a significant advance in both spatial coverage and validation intensity. Building on the 2024 pilot surveys and test excavations, expanded magnetometry in 2025 enabled assessment of anomaly continuity and patterning across a larger set of grids/sectors in the northwestern portion of the site. Magnetometry-guided verification—including shallow test

excavations in additional sectors—provided distributed ground-truth anchors that corroborate the anthropogenic nature of high-amplitude anomalies and refine the functional interpretation of production-related areas. This progression from "initial confirmation" (2024) to "systematic cross-checking over broader coverage" (2025) highlights the scalability of the workflow for large and complex settlements.

Across both seasons, GNSS-PPP served as the geodetic backbone, ensuring interoperability and precise alignment among datasets acquired at different resolutions and by different sensors. The resulting georeferenced products—updated composite plan, UAV-derived models, and anomaly maps—form a robust foundation for planning future excavation strategies, defining priority areas, and supporting long-term monitoring and site management.

Despite these advances, the archaeological excavations conducted in 2024–2025 were intentionally limited in depth and extent, serving primarily as verification tests. Consequently, documenting deeper stratigraphic sequences, secure absolute dating, and broader material-culture and ecofactual datasets remain priorities for future field seasons. Future work should therefore focus on: (i) expanded stratigraphic excavations in selected areas where remote sensing and geophysics indicate coherent architectural units; (ii) systematic sampling for chronometric control (including datable organics where available and diagnostic ceramic assemblages); (iii) a stronger integration of artefact, archaeometric, and bioarchaeological analyses to address chronology, economy, and the evolution of functional zoning between the 1st and 5th centuries AD; and (iv) an evidence-weighted, multiscale–multitemporal synthesis based on a confidence ("historical reliability") scale, integrating Soviet-era plans, satellite/UAV observations, and geophysics into uncertainty-aware interpretative mapping of the site's urban layout and functional zones.

Finally, the project demonstrates the value of open, integrative geomatics for archaeological research in Central Asia. Incorporating the results into a structured GIS/geodatabase and web-based visualization environment supports transparent interpretation, reproducibility, and incremental updating as new data is collected. In the near future, the workflow may be further enhanced by introducing machine-learning approaches to assist in the semi-automated detection and classification of anthropogenic patterns across large image and geophysical datasets (e.g., feature extraction, anomaly clustering, and probabilistic mapping), while maintaining ground-truth verification as the decisive interpretative step. Overall, Zar Tepe provides a transferable model for multi-sensor archaeological prospection and interpretation in arid landscapes where excavation must be carefully targeted and optimized.

Author Contributions: Conceptualization, J.A., P.U., V.M.-F., C.I., J.M.G., A.Z., I.Y., U.M., H.H., E.A., C.V. and S.R.P.; Methodology, P.U., J.A., C.I., V.M.-F., J.M.G., E.A., A.Z., I.Y., U.M., H.H., C.V. and S.R.P.; Software, J.A., P.U., C.I., A.Z., I.Y., U.M., H.H. and C.V.; Validation, J.A., P.U., V.M.-F., C.I., J.M.G., E.A., A.Z., I.Y., U.M., H.H., C.V. and S.R.P.; Formal analysis, J.A., P.U., C.I., A.Z., I.Y., U.M., H.H. and C.V.; Investigation, J.A., P.U., V.M.-F., C.I., J.M.G., E.A., A.Z., I.Y., U.M., H.H., C.V. and S.R.P.; Resources, J.A., P.U., V.M.-F., C.I., E.A., J.M.G., A.Z., I.Y., U.M., H.H., C.V. and S.R.P.; Data curation, J.A., P.U., C.I., V.M.-F., J.M.G., E.A., A.Z., I.Y., U.M., H.H., C.V. and S.R.P.; Writing—original draft preparation, J.A., P.U., C.I., V.M.-F., J.M.G., E.A., A.Z., I.Y., U.M., H.H. and C.V.; Writing—review and editing, J.A., P.U., C.I., V.M.-F., E.A., J.M.G., A.Z., I.Y., U.M., H.H., C.V. and S.R.P.; Visualization, J.A., P.U., C.I., A.Z., I.Y., U.M., H.H. and C.V.; Supervision, J.A., P.U., V.M.-F., J.M.G., A.Z., H.H., E.A. and S.R.P.; Project administration, P.U., V.M.-F., J.A., J.M.G., E.A. and S.R.P.; Funding acquisition, P.U., V.M.-F., J.A., C.I., A.Z., I.Y., U.M., H.H. and S.R.P. All authors have read and agreed to the published version of the manuscript.

Funding: This research was funded by several research projects supported by the Spanish Ministry of Science and Innovation, led by Paula Uribe; PID2024-157190NB-C22, co-led by Paula Uribe and Jorge Angás; and PID2020-114096GB-C21 and PID2024-157190NB-C21, led by Verónica Martínez-Ferreras. Additional funding was provided through the DiGHER research project (CPP2022-009631), led by Jorge Angás and funded by MCIU/AEI/10.13039/501100011033 and by the European Union's NextGenerationEU/PRTR program. The Spanish Palarq Foundation contributed to supporting the archaeological fieldwork conducted in Zar Tepe in 2024 and 2025, led by Verónica Martínez-Ferreras. Cristian Iranzo contributed to this study through a PhD research contract funded by the Department of Science, University and Knowledge Society of the Government of Aragón (Spain).

Institutional Review Board Statement: Not applicable.

Informed Consent Statement: Not applicable.

Data Availability Statement: The data presented in this study are not publicly available due to legal restrictions, heritage protection requirements, and the sensitive nature of archaeological site-location information. The authors are not authorized to share or redistribute these data.

Acknowledgments: The authors would like to acknowledge Alberto Gómez and Agustín López from Leica Geosystems Barcelona (part of the Hexagon Group) for the availability and temporary provision of both software and hardware, specifically the Leica GS07 GNSS receiver, which was used for fieldwork during this study. The authors also acknowledge the technical support provided for the different tests conducted in relation to field-based topographic layout and the georeferencing of anomalies detected through remote sensing and geophysical survey, using the GNSS Precise Point Positioning (PPP) system. The authors also wish to thank Fernando Pérez-Cabello for his valuable advice and guidance on satellite image processing.

Conflicts of Interest: The authors declare no conflicts of interest.

Abbreviations

The following abbreviations are used in this manuscript:

BOA	Bottom-of-Atmosphere
CNN	Convolutional Neural Network
CORS	Continuously Operating Reference Stations
DEM	Digital Elevation Model
DSM	Digital Surface Model
DTM	Digital Terrain Model
FAIR	Findable, Accessible, Interoperable, Reusable
GCP	Ground Control Point
GDAL	Geospatial Data Abstraction Library
GEMI	Global Environmental Monitoring Index
GNSS	Global Navigation Satellite System
GSD	Ground Sampling Distance
LoG	Laplacian of Gaussian
NIR	Near-Infrared
OSAVI	Optimized Soil-Adjusted Vegetation Index
OTB	Orfeo ToolBox
PCA	Principal Component Analysis
PDAL	Point Data Abstraction Library
PPP	Precise Point Positioning
proj4js	Proj4 JavaScript library (coordinate transformations)
RMSE	Root Mean Square Error
RTK	Real-Time Kinematic
SfM	Structure from Motion
three.js	three.js JavaScript 3D library
UAV	Unmanned Aerial Vehicle

UZPOS	Uzbekistan national CORS/positioning network
WebGL	Web Graphics Library
WV3	WorldView-3
Py6S	Python interface to the 6S radiative transfer model

Appendix A



Figure A1. Integrated satellite-to-ground methodological workflow applied at Zar Tepe. The workflow starts from the main archaeological prospection objectives and follows an iterative laboratory–field–laboratory–field sequence. Legacy documentation, CORONA/HEXAGON and WorldView-3 imagery were first integrated to detect potential archaeological anomalies. UAV photogrammetry, GNSS-PPP spatial control, magnetometry and targeted test excavations were then used to refine, validate and interpret these anomalies. The final outputs were integrated into a relational GIS geodatabase and the DiGHER platform to support the updated site plan, urban-layout interpretation and the definition of future excavation priorities.

References

1. Leriche, P. Bactria, Land of a Thousand Cities. In *After Alexander: Central Asia Before Islam*; Cribb, J., Herrmann, G., Eds.; The British Academy: London, UK, 2007; Volume 133, pp. 121–153. [CrossRef]
2. Stride, S. Regions and Territories in Southern Central Asia: What the Surkhan Darya Province Tells Us about Bactria. In *After Alexander: Central Asia Before Islam*; Cribb, J., Herrmann, G., Eds.; Proceedings of the British Academy; British Academy: London, UK, 2007; Volume 133, pp. 99–117. [CrossRef]
3. Benjamin, C. *Empires of Ancient Eurasia: The First Silk Roads Era, 100 BCE—250 CE*, 1st ed.; Cambridge University Press: Cambridge, UK, 2018; ISBN 978-1-107-53543-5.
4. Mukhamedjanov, A.R. Economy and Social System in Central Asia in the Kushan Age. In *History of Civilizations of Central Asia*; Harmatta, J., Puri, B.N., Etemadi, G.F., Eds.; UNESCO Publishing: Paris, France, 1994; Volume 2, pp. 265–290.
5. Mkrtychev, T. Buddhism and Features of the Buddhist Art of Bactria-Tokharistan. In *After Alexander: Central Asia Before Islam*; Cribb, J., Herrmann, G., Eds.; British Academy: London, UK, 2007; Volume 133, pp. 475–485. [CrossRef]
6. Baumer, C. *The History of Central Asia; The Age of the Silk Roads*; I.B. Tauris: London, UK; New York, NY, USA, 2014; Volume 2.
7. Beckwith, C.I. *Empires of the Silk Road: A History of Central Eurasia from the Bronze Age to the Present*; Princeton University Press: Princeton, NJ, USA, 2009; ISBN 978-0-691-13589-2.
8. Khamidov, M.; Ishchanov, J.; Hamidov, A.; Donmez, C.; Djumaboev, K. Assessment of Soil Salinity Changes under the Climate Change in the Khorezm Region, Uzbekistan. *Int. J. Environ. Res. Public Health* **2022**, *19*, 8794. [CrossRef] [PubMed]
9. Ariño, E.; Uribe, P.; Angás, J.; Piqué, R.; Portero, R.; Martínez-Ferreras, V.; Gurt, J.M. Adaptive Dynamics of Settlement Models in the Urban Landscape of Termez (Uzbekistan) from c. 300 BCE to c. 1400 CE. *Land* **2023**, *12*, 1550. [CrossRef]
10. Zavyalov, V.A. *Kushanshakhr pri Sasanidakh (po Matyerialam Raskopok Gorodishcha Zartepa)/Kushanhahr Under the Sasanian (on the Results of Excavations of the Zartepa Site)*; St. Petersburg State University, Faculty of Philology and Arts: St. Petersburg, Russia, 2008.
11. Sabirov, K.S. Kushanskaya fortifikatsiya v svyetye raskopok na gorodishchye Zar-Tepe. In *Baktriyskiye Dryevnosti: Pryedvarityelnyye Coobshchyeniya ob Arkhyeologichyeskikh Rabotakh na Yugye Uzbekistana*; Nauka: Leningrad, Russia, 1976; pp. 46–50.
12. Pidaev, S.R. Dva klada monyet postkushanskogo vryemyeny iz Cyevyernoy Baktrii. In *Gorodskaya Sryeda i Cultura Baktrii-Tokharistana i Sogda (IV v. do n. e.-VIII v. n. e.): Tyezisy Dokladov Covyetsko-Frantsuzkogo Kollokviuma, Samarkand, Uzbekistan, 25–30 August 1986*; Fan: Tashkent, Uzbekistan, 1986; pp. 77–78.
13. Gurt Esparraguera, J.M.; Pidaev, S.R.; Rauret, A.M.; Stride, S. *Preliminary Report of the Work of the International Pluridisciplinary Archaeological Expedition to Bactria 2006*; IPAEB: Barcelona, Spain, 2007.
14. Gurt Esparraguera, J.M.; Pidaev, S.R.; Rauret, A.M.; Stride, S. *Preliminary Report of the Work of the International Pluridisciplinary Archaeological Expedition to Bactria 2007*; IPAEB: Barcelona, Spain, 2008.
15. Gurt Esparraguera, J.M.; Pidaev, S.R.; Rauret, A.M.; Stride, S. *Preliminary Report of the Work of the International Pluridisciplinary Archaeological Expedition to Bactria 2008*; IPAEB: Barcelona, Spain, 2009.
16. Gurt Esparraguera, J.M.; Pidaev, S.R.; Rauret, A.M.; Stride, S. *Preliminary Report of the Work of the International Pluridisciplinary Archaeological Expedition to Bactria 2009*; IPAEB: Barcelona, Spain, 2010.
17. Gurt Esparraguera, J.M.; Pidaev, S.R. *Preliminary Report of the Work of the International Pluridisciplinary Archaeological Expedition to Bactria 2010*; IPAEB: Barcelona, Spain, 2011.
18. Fusaro, A.; Gurt Esparraguera, J.M.; Ariño Gil, E.; Uribe Agudo, P.; Angás Pajas, J.; Pidaev, S.R. Islamic Ancient Termez: An Active and Long-Established Ceramic Manufacturing Centre along the Silk Road. *Archaeol. Res. Asia* **2022**, *31*, 100375. [CrossRef]
19. Martínez, V.; Ariño, E.; Gurt, J.M.; Pidaev, S. The Enclosure of Tchingiz-Tepe (Ancient Termez, Uzbekistan) during the Kushan and Kushan-Sassanian Periods: Archaeological Stratigraphy and 14C Dating Analyses. *Iran. Antiq.* **2014**, *49*, 413–469. [CrossRef]
20. Angás, J.; Uribe, P.; Ariño, E.; Gurt, J.M.; Martínez-Ferreras, V.; Pidaev, S. A Multi-Scalar Photogrammetric Recording Approach in Termez (Uzbekistan). *Int. Arch. Photogramm. Remote Sens. Spat. Inf. Sci.* **2019**, *XLII-2-W15*, 93–100. [CrossRef]
21. Angás, J.; Uribe, P.; Bea, M.; Farjas, M.; Ariño, E.; Martinez-Ferreras, V.; Gurt, J.M. Potential of CORONA Satellite Imagery for 3D Reconstruction of Archaeological Landscapes. In *Proceedings of the 3rd Congress in Geomatics Engineering*; CIGeo: Valencia, Spain, 2021; pp. 35–41. [CrossRef]
22. Iranzo, C.; Uribe Agudo, P.; Angas, J.; Ariño Gil, E.; Martínez Ferreras, V.; Gurt, J.M.; Pidaev, S.R. Archaeological Prospection with Corona and Wv-3 Satellite Imagery of the Archaeological Site of Zar Tepe (Uzbekistan). *Int. Arch. Photogramm. Remote Sens. Spat. Inf. Sci.* **2023**, *XLVIII-M-2–2023*, 743–749. [CrossRef]
23. Shchetenko, A.Y. Raskopki monumyentalnogo arkhityekturnogo komplyeksa Zar-tepe. In *Drevnyaya Baktriya: Pryedvarityelnyye Coobshchyeniya ob Arkhyeologichyeskikh Rabotakh na Yugye Uzbekistana*; Nauka: Leningrad, Russia, 1974; pp. 42–48.
24. Sabirov, K.S.; Pilipko, V.N. Raskopki oboronityelnykh sooruzhyeniy gorodishcha Zar-tepe. In *Drevnyaya Baktriya: Pryedvarityelnyye Coobshchyeniya ob Arkhyeologichyeskikh Rabotakh na Yugye Uzbekistana*; Nauka: Leningrad, Russia, 1974; pp. 49–53.
25. Pilipko, V.N. Raskopki svyatilishcha pozdnyekushanskogo vryemyeny na gorodishchye Zar-Tepe. In *Baktriyskiye Dryevnosti: Pryedvarityelnyye Coobshchyeniya ob Arkhyeologichyeskikh Rabotakh na Yugye Uzbekistana*; Nauka: Leningrad, Russia, 1976; pp. 59–68.

26. Zavyalov, V.A.; Osipov, V.I. Raskopki zhilogo komplyeksa na gorodishchye Zar-Tepe v 1973 g. In *Baktriyskiye Dryevnosti: Pryedvarityelnyye Coobshchyeniya ob Arkhyeologichyeskikh Rabotakh na Yugye Uzbekistana*; Nauka: Leningrad, Russia, 1976; pp. 51–58.
27. Masson, V.M. Problyema dryevnyego goroda i arkhyeologichyeskiye pamyatniki Cyevyernoy Baktrii (Pyerspyectivy isslyedovaniya). In *Drevnyaya Baktriya: Pryedvarityelnyye Coobshchyeniya ob Arkhyeologichyeskikh Rabotakh na Yugye Uzbekistana*; Nauka: Leningrad, Russia, 1974; pp. 3–13.
28. Zavyalov, V.A. Raskopki kvartala pozdnyekushanskogo vryemyeny na gorodishchye Zartepe v 1975–1976 gg. *Sov. Arkhyeologiya* **1979**, *3*, 141–154.
29. Zavyalov, V.A. Pozdnyekushanskaya antropomorfnaya tyerrakota Zartepe. *Kratk. Soobshcheniya Instituta Arkheologii* **1981**, *167*, 65–69.
30. Zavyalov, V.A.; Galibin, V.A. Bronzovaya posuda pozdnyekushanskogo vryemyeny iz Zar-tepe. *Kratk. Soobshcheniya Instituta Arkheologii* **1990**, *199*, 95–101.
31. Zavyalov, V.A. Kostyanyye pryedmyety tualyeta iz pamyatnikov Sryednyey Azii kushanskogo i postkushanskogo vryemyeny. *Kratk. Soobshcheniya Instituta Arkheologii* **1993**, *209*, 31–41.
32. Abdullaev, K.; Zavyalov, V.A. Buddiyskiye motivy v gorodckoy kulturye pozdnyekushanskogo vryemyeny (Po matyerialam Zar-tepe). *Vyestnik Dryevnyey Istor.* **1985**, *4*, 111–121.
33. Abdullaev, K.; Zavyalov, V.A. Sosudy na zoomorfnyx podstavkakh iz posyetsyeniy kushanskoy Bactrii. *Sov. Arkhyeologiya* **1985**, *1*, 202–211.
34. Pidaev, S.R. Arkhyeologichyeskiye raboty na yugo-vostochnom kholmye Zartepa. *Istor. Matyerialnoy Kult. Uzb.* **1990**, *24*, 50–60.
35. Reutova, M.A. Zhivopis Zar-tepa. *Istor. Matyerialnoy Kult. Uzb.* **1986**, *25*, 193–197.
36. Pidaev, S.R. Raskopki zhilogo komplyeksa v syevyero-zapadnoy chasti gorodishcha Zartepa. *Istor. Matyerialnoy Kult. Uzb.* **1988**, *22*, 34–44.
37. Abdullaev, K.; Annaev, T. Raskopki na gorodishchye Zartepa v 1979–1981 gg. *Istor. Matyerialnoy Kult. Uzb.* **1990**, *23*, 12–25.
38. Casana, J. Global-Scale Archaeological Prospection Using CORONA Satellite Imagery: Automated, Crowd-Sourced, and Expert-Led Approaches. *J. Field Archaeol.* **2020**, *45*, S89–S100. [CrossRef]
39. Ur, J.A. CORONA Satellite Imagery and Ancient Near Eastern Landscapes. In *Mapping Archaeological Landscapes from Space*; Comer, D.C., Harrower, M.J., Eds.; Springer: New York, NY, USA, 2013; pp. 21–31. ISBN 978-1-4614-6074-9.
40. Watanabe, N.; Nakamura, S.; Liu, B.; Wang, N. Utilization of Structure from Motion for Processing CORONA Satellite Images: Application to Mapping and Interpretation of Archaeological Features in Liangzhu Culture, China. *Archaeol. Res. Asia* **2017**, *11*, 38–50. [CrossRef]
41. Mantellini, S.; Berdimuradov, A.E. Evaluating the Human Impact on the Archaeological Landscape of Samarkand (Uzbekistan): A Diachronic Assessment of the Taylak District by Remote Sensing, Field Survey, and Local Knowledge. *Archaeol. Res. Asia* **2019**, *20*, 100143. [CrossRef]
42. Vanonckelen, S.; Lhermitte, S.; Van Rompaey, A. The Effect of Atmospheric and Topographic Correction Methods on Land Cover Classification Accuracy. *Int. J. Appl. Earth Obs. Geoinf.* **2013**, *24*, 9–21. [CrossRef]
43. Opitz, R.; Herrmann, J. Recent Trends and Long-Standing Problems in Archaeological Remote Sensing. *J. Comput. Appl. Archaeol.* **2018**, *1*, 19–41. [CrossRef]
44. Agapiou, A. Remote Sensing Heritage in a Petabyte-Scale: Satellite Data and Heritage Earth Engine© Applications. *Int. J. Digit. Earth* **2017**, *10*, 85–102. [CrossRef]
45. Ghuffar, S.; Bolch, T.; Rupnik, E.; Bhattacharya, A. A Pipeline for Automated Processing of Declassified Corona KH-4 (1962–1972) Stereo Imagery. *IEEE Trans. Geosci. Remote Sens.* **2022**, *60*, 5629614. [CrossRef]
46. Wilson, R.T. Py6S: A Python Interface to the 6S Radiative Transfer Model. *Comput. Geosci.* **2013**, *51*, 166–171. [CrossRef]
47. Marcello, J.; Eugenio, F.; Perdomo, U.; Medina, A. Assessment of Atmospheric Algorithms to Retrieve Vegetation in Natural Protected Areas Using Multispectral High Resolution Imagery. *Sensors* **2016**, *16*, 1624. [CrossRef] [PubMed]
48. Martin, J.; Eugenio, F.; Marcello, J.; Medina, A.; Bermejo, J.A.; Arbelo, M. Atmospheric Correction Models for High Resolution WorldView-2 Multispectral Imagery: A Case Study in Canary Islands, Spain. In *Remote Sensing of Clouds and the Atmosphere XVII; and Lidar Technologies, Techniques, and Measurements for Atmospheric Remote Sensing VIII*; Kassianov, E.I., Comeron, A., Picard, R.H., Schäfer, K., Singh, U.N., Pappalardo, G., Eds.; SPIE: Bellingham, WA, USA, 2012; Volume 8534, pp. 153–162. [CrossRef]
49. Zhang, K.; Zhang, F.; Wan, W.; Yu, H.; Sun, J.; Del Ser, J.; Elyan, E.; Hussain, A. Panchromatic and Multispectral Image Fusion for Remote Sensing and Earth Observation: Concepts, Taxonomy, Literature Review, Evaluation Methodologies and Challenges Ahead. *Inf. Fusion* **2023**, *93*, 227–242. [CrossRef]
50. Wu, Z.-C.; Huang, T.-Z.; Deng, L.-J.; Huang, J.; Chanussot, J.; Vivone, G. LRTCFPan: Low-Rank Tensor Completion Based Framework for Pansharpening. *IEEE Trans. Image Process.* **2023**, *32*, 1640–1655. [CrossRef] [PubMed]
51. Kalayci, T.; Lasaponara, R.; Wainwright, J.; Masini, N. Multispectral Contrast of Archaeological Features: A Quantitative Evaluation. *Remote Sens.* **2019**, *11*, 913. [CrossRef]

52. Abouarab, M.A.R.; Ibrahim, A.; Eldosouky, A.M.; Aboalkassim, I.; Younes, A.; El-Qady, G.; Abbas, A.M.; El-hemaly, I.A.; Awad, A.; Wilson, P.; et al. Identification of Architectural Roman Remains in the Complex Archaeological Site of Buto 'Tell El Fara'in', Northern Egypt, Using Geophysical and Remote Sensing Data. *Archaeol. Prospect.* **2025**, *32*, 437–457. [CrossRef]
53. Iranzo, C. *CristianICS/ArqPy-Processing: ArcPy Toolbox-1.0.1*; Zenodo: Geneva, Switzerland, 2026. [CrossRef]
54. Grizonnet, M.; Michel, J.; Poughon, V.; Inglada, J.; Savinaud, M.; Cresson, R. Orfeo ToolBox: Open Source Processing of Remote Sensing Images. *Open Geospat. Data Softw. Stand.* **2017**, *2*, 15. [CrossRef]
55. Pugachenkova, G.A. Kvartal kyeramistov (Dt-9). In *Dalverzintepe: Kushanskiy Gorod na Yugye Uzbyekistana*; Pugachenkova, G.A., Rtveladze, E.V., Eds.; Fan, Academy of Sciences of the Soviet Socialist Republic of Uzbekistan: Tashkent, Uzbekistan, 1978; pp. 115–143.
56. Tsantini, E.; Martínez Ferreras, V.; Ariño Gil, E.; Gurt I Esparraguera, J.M.; Pidaev, S. Pottery Production in the Buddhist Communities in Central Asia: The Kushan-Sassanian Pottery Workshop of Kara Tepe (Termez, Uzbekistan). *Archaeometry* **2016**, *58*, 35–56. [CrossRef]

Disclaimer/Publisher's Note: The statements, opinions and data contained in all publications are solely those of the individual author(s) and contributor(s) and not of MDPI and/or the editor(s). MDPI and/or the editor(s) disclaim responsibility for any injury to people or property resulting from any ideas, methods, instructions or products referred to in the content.